

12

# FERROELECTRIC TUNGSTEN BRONZE BULK CRYSTALS AND EPITAXIAL THIN FILMS FOR ELECTRO-OPTIC DEVICE APPLICATIONS

AD-A145 577

Semi-Annual Technical Report No. 3  
For Period 10/1/83 through 3/31/84

JULY 1984

|                             |   |
|-----------------------------|---|
| DARPA Order No.             | 4540  |
| Program Code:               | P2D10   |
| Name of Contractor:         | Rockwell International Corporation  |
| Effective Date of Contract: | 09/30/82  |
| Contract Expiration Date:   | 09/29/85  |
| Amount of Contract Dollars: | \$1,051,699   |
| Contract Number:            | N00014-82-C-2466  |
| Principal Investigators:    | Dr. R.R. Neurgaonkar<br>(805) 498-4545, Ext. 109<br><br>Dr. L.E. Cross<br>Pennsylvania State University<br>(814) 865-1181 |

Sponsored by

Defense Advanced Research Projects Agency (DoD)  
DARPA Order No. 4540  
Monitored by Naval Research Laboratory  
Under Contract No. N00014-82-C-2466

SEP 17 1984

The views and conclusions contained in this document are those of the authors and should not be interpreted as necessarily representing the official policies, either expressed or implied, of the Defense Advanced Research Projects Agency or the United States Government.

Approved for public release; distribution unlimited.

84 09 14 001

DTIC FILE COPY

## REPORT DOCUMENTATION PAGE

|  |  |  |   |
|--|--|--|---|
| 1a REPORT SECURITY CLASSIFICATION<br>Unclassified  |  | 1b RESTRICTIVE MARKINGS  |   |
| 2a SECURITY CLASSIFICATION AUTHORITY   |  | 3. DISTRIBUTION/AVAILABILITY OF REPORT<br>Approved for public release; distribution unlimited.   |   |
| 2b DECLASSIFICATION/DOWNGRADING SCHEDULE   |  |  |   |
| 4 PERFORMING ORGANIZATION REPORT NUMBER(S)<br>SC5340.6SA   |  | 5. MONITORING ORGANIZATION REPORT NUMBER(S)  |   |
| 6a. NAME OF PERFORMING ORGANIZATION<br>Rockwell International<br>Science Center  | 6b. OFFICE SYMBOL<br>(If applicable)         | 7a. NAME OF MONITORING ORGANIZATION<br>Defense Advanced Research Projects Agency   |   |
| 6c. ADDRESS (City, State and ZIP Code)<br>1049 Camino Dos Rios<br>Thousand Oaks, California 91360  |  | 7b. ADDRESS (City, State and ZIP Code)<br>1400 Wilson Boulevard<br>Arlington, VA 22209   |   |
| 8a. NAME OF FUNDING/SPONSORING ORGANIZATION<br>Naval Research Laboratory   | 8b. OFFICE SYMBOL<br>(If applicable)         | 9. PROCUREMENT INSTRUMENT IDENTIFICATION NUMBER<br>Contract No. N00014-82-C-2466   |   |
| 8c. ADDRESS (City, State and ZIP Code)<br>4555 Overlook Avenue S.W.<br>Washington, DC 20375  |  | 10 SOURCE OF FUNDING NOS   |   |
|  |  | PROGRAM ELEMENT NO   | PROJECT NO.<br>DARPA<br>Order No.<br>4540 |
|  |  | TASK NO  | WORK UNIT NO                              |
| 11. TITLE (Include Security Classification) FERROELECTRIC TUNGSTEN BRONZE BULK CRYSTALS AND EPITAXIAL THIN FILMS FOR ELECTRO-OPTIC DEVICE APPLICATIONS   |  |  |   |
| 12. PERSONAL AUTHOR(S)<br>Cross, Dr. L.E.; Oliver, J.R.; Naurgaonkar, Dr. R.R.   |  |  |   |
| 13a. TYPE OF REPORT<br>Semi-Annual Tech Rpt #3   | 13b. TIME COVERED<br>FROM 10/1/83 TO 3/31/84 | 14. DATE OF REPORT (Yr., Mo., Day)<br>JULY 1984  | 15. PAGE COUNT<br>48                      |
| 16. SUPPLEMENTARY NOTATION<br>The views and conclusions contained in this document are those of the authors and should not be interpreted as necessarily representing the official policies, either expressed or implied, of the Defense Advanced Research Projects Agency of the U.S. Government.   |  |  |   |
| 17. COSATI CODES   |  | 18. SUBJECT TERMS (Continue on reverse if necessary and identify by block number)  |   |
| FIELD  | GROUP  | SBN, PBN, PKN, BNN, SNN, Morphotropic Phase Boundary, Tungsten Bronze, Striations, E-O Coefficient, LPE Flux, Dielectric Constant, Writing Sensitivity, Ca, Fe Dopants |   |
|  |  |  |   |
| 19. ABSTRACT (Continue on reverse if necessary and identify by block number)<br>Several doped ( $Fe^{3+}$ and $Ce^{3+}$ ) and undoped SBN:60 single crystals have been grown by the Czochralski technique. Although the quality of doped crystals needs to be improved, they show a considerable enhancement in electro-optic and photorefractive properties, specifically for $Ce^{3+}$ -doped SBN:60 crystals. The addition of these impurity species did not change the growth conditions significantly; however, striations were present and became stronger as the concentration of impurity ions increased. Undoped SBN:60 single crystals have also been grown and they are almost striation-free and exhibit excellent electro-optic properties.<br><br>Phase diagram work on the system $SrV_2O_6$ - $BaV_2O_6$ - $SrNb_2O_6$ - $BaNb_2O_6$ has determined that SBN:75 films can be grown from flux compositions which cover a relatively limited range in the phase diagram. Work on the pseudo-binary flux systems $BaV_2O_6$ -PBN:60 and $Pb_{1-x}Ba_xNb_2O_6$ -PBN:60 for PBN film growth has resulted in the formation of the tetragonal PBN phase for one composition, a highly encouraging result.<br><br>Research has continued on the pseudo-binary morphotropic bronze systems $Ba_2NaNb_5O_{15}$ - $Sr_2NaNb_5O_{15}$ (BNN-SNN) and $Pb_2KNb_5O_{15}$ - $Ba_2NaNb_5O_{15}$ (PKN-BNN). Improved sintering of ceramic compositions |  |  |   |
| 20. DISTRIBUTION/AVAILABILITY OF ABSTRACT<br>UNCLASSIFIED/UNLIMITED <input checked="" type="checkbox"/> SAME AS RPT. <input type="checkbox"/> DTIC USERS <input type="checkbox"/>  |  | 21. ABSTRACT SECURITY CLASSIFICATION<br>Unclassified   |   |
| 22a. NAME OF RESPONSIBLE INDIVIDUAL  | 22b. TELEPHONE NUMBER<br>(Include Area Code) | 22c. OFFICE SYMBOL   |   |



TABLE OF CONTENTS

|  | <u>Page</u> |
|--|-------------|
| 1.0 SUMMARY AND PROGRESS.....  | 1           |
| 2.0 DEVELOPMENT OF OPTICAL QUALITY SBN:60.....   | 3           |
| 2.1 Materials Growth Techniques.....   | 3           |
| 2.2 Growth Procedure.....  | 3           |
| 2.3 Growth of Undoped SBN:60 Crystals.....   | 5           |
| 2.4 Growth of Doped SBN:60 Crystals.....   | 5           |
| 3.0 LIQUID PHASE EPITAXIAL GROWTH OF BRONZE COMPOSITIONS.....  | 12          |
| 3.1 Flux Systems for SBN:75.....   | 12          |
| 3.2 Flux Systems for PBN:60.....   | 16          |
| 4.0 NEW TUNGSTEN BRONZE SYSTEMS FOR ELECTRO-OPTIC STUDIES.....   | 20          |
| 4.1 Ba <sub>2</sub> NaNb <sub>5</sub> O <sub>15</sub> -Sr <sub>2</sub> NaNb <sub>5</sub> O <sub>15</sub> System..... | 20          |
| 4.2 Pb <sub>2</sub> KNb <sub>5</sub> O <sub>15</sub> -Ba <sub>2</sub> NaNb <sub>5</sub> O <sub>15</sub> System.....  | 25          |
| 5.0 OPTICAL EVALUATION OF PBN.....   | 29          |
| 5.1 Introduction.....  | 29          |
| 5.2 Exploratory Measurements.....  | 30          |
| 6.0 EVALUATION OF THE PHOTOREFRACTIVE EFFECT IN DOPED AND<br>UNDOPED SBN:60.....                                     | 34          |
| 6.1 Introduction.....  | 34          |
| 6.2 Photorefractive Measurements.....  | 36          |
| 7.0 FUTURE PLANNED WORK.....   | 41          |
| 8.0 PUBLICATIONS AND PRESENTATIONS.....  | 42          |
| 8.1 Publications.....  | 42          |
| 8.2 Presentations.....   | 42          |
| 9.0 REFERENCES.....  | 43          |



LIST OF FIGURES

|   | <u>Page</u> |
|---|-------------|
| Fig. 1 Ce-doped SBN:60 crystals grown by the Czochralski method.....  | 10          |
| Fig. 2 Quaternary phase diagram of the SrO-BaO-Nb <sub>2</sub> O <sub>5</sub> -V <sub>2</sub> O <sub>5</sub> system....   | 13          |
| Fig. 3 Quaternary phase diagram of the SrV <sub>2</sub> O <sub>6</sub> -BaV <sub>2</sub> O <sub>6</sub> -SrNb <sub>2</sub> O <sub>6</sub> -BaNb <sub>2</sub> O <sub>6</sub> system.....                       | 15          |
| Fig. 4 Quaternary phase diagram of the Pb <sub>2</sub> V <sub>2</sub> O <sub>7</sub> -PbNb <sub>2</sub> O <sub>6</sub> -BaNb <sub>2</sub> O <sub>6</sub> system.....  | 18          |
| Fig. 5 Quaternary phase diagram of PbV <sub>2</sub> O <sub>6</sub> -BaV <sub>2</sub> O <sub>6</sub> -PbNb <sub>2</sub> O <sub>6</sub> -BaNb <sub>2</sub> O <sub>6</sub> system.....                           | 19          |
| Fig. 6 Morphotropic phase boundary conditions for the system BNN-SNN.....   | 22          |
| Fig. 7 Dielectric constant (at 10 kHz) vs composition for the system BNN-SNN.....   | 22          |
| Fig. 8 Dielectric constant of ceramic Sr <sub>2</sub> NaNb <sub>5</sub> O <sub>15</sub> (SNN) as a function of temperature.....   | 23          |
| Fig. 9 Morphotropic phase boundary conditions for the system PKN-BNN.....   | 26          |
| Fig. 10 Dielectric constant (at 10 kHz) vs composition for the system PKN-BNN.....  | 26          |
| Fig. 11 Dielectric constant of ceramic PKN, 0.8 PKN-0.2 BNN and BNN as a function of temperature. Data for BNN is expanded by a factor of 10 for clarity.....   | 27          |
| Fig. 12 Structural lattice parameters as a function of composition for PKN-BNN. Note the abrupt discontinuity for the <u>b</u> and <u>c</u> parameters at the morphotropic 0.75 PKN-0.25 BNN composition..... | 28          |
| Fig. 13 K vs T measurement along the a, b and c axes of orthorhombic PBN (composition near the morphotropic boundary).....  | 31          |





LIST OF TABLES

| Table |   | <u>Page</u> |
|-------|---|-------------|
| 1     | Materials for Bulk Single Crystal SBN:60 Growth.....                    | 4           |
| 2     | Growth of SBN Single Crystals.....                                      | 6           |
| 3     | Impurities in Starting Chemicals Used for SBN:60 Crystals....           | 7           |
| 4     | Proposed Dopants for Photorefractive SBN and Other Bronze Crystals..... | 8           |
| 5     | Growth Data on Doped and Undoped SBN:60 Crystals.....                   | 9           |
| 6     | LPE Fluxes for SBN.....   | 14          |
| 7     | LPE Fluxes for PBN.....   | 17          |
| 8     | Dielectric Properties of Hot-Pressed BNN-SNN.....                       | 24          |
| 9     | Optical Properties of Doped and Undoped SBN:60 crystals.....            | 40          |



## 1.0 SUMMARY AND PROGRESS

The tungsten bronze structural family has been shown to be useful for a number of applications, including electro-optic, nonlinear optical and pyroelectric applications. The current work reports the development of optical quality  $\text{Sr}_{1-x}\text{Ba}_x\text{Nb}_2\text{O}_6$  ( $x = 0.40$ ) for electro-optic and photorefractive device studies. Considerable progress has been made in different areas, including the growth of doped SBN:60 single crystals and LPE films, as well as electro-optic and photorefractive characterization.

Several doped ( $\text{Fe}^{3+}$  and  $\text{Ce}^{3+}$ ) and undoped SBN:60 single crystals have been grown by the Czochralski technique. Although the quality of doped crystals needs to be improved, they show a considerable enhancement in electro-optic and photorefractive properties, specifically for  $\text{Ce}^{3+}$ -doped SBN:60 crystals. The addition of these impurity species did not change the growth conditions significantly; however, striations were present and became stronger as the concentration of impurity ions increased. Once suitable dopants and dopant concentrations are optimized for photorefractive studies, effort will be extended to improve the crystal quality and size. Undoped SBN:60 single crystals have also been grown and the quality of these crystals is consistent, i.e., they are almost striation-free and exhibit excellent electro-optic properties. In order to improve the optical quality of these SBN:60 crystals, higher grade starting materials are now being used for this growth. The results of this work are promising and will be discussed in our next report.

Extensive work has been performed on the flux systems required for LPE thin film growth of SBN and  $\text{Pb}_{1-x}\text{Ba}_x\text{Nb}_2\text{O}_6$  (PBN) bronze compositions. Phase diagram work on the system  $\text{SrV}_2\text{O}_6$ - $\text{BaV}_2\text{O}_6$ - $\text{SrNb}_2\text{O}_6$ - $\text{BaNb}_2\text{O}_6$  has determined that SBN:75 films can be grown from flux compositions which cover a relatively limited range in the phase diagram, and with a relatively high melting point ( $> 1350^\circ\text{C}$ ). Work on the flux system  $\text{Pb}_2\text{V}_2\text{O}_7$ - $\text{Ba}_2\text{V}_2\text{O}_7$ - $\text{PbNb}_2\text{O}_6$ - $\text{BaNb}_2\text{O}_6$  showed that only the rhombohedral PBN phase could be precipitated, even when quenching to room temperature from  $1250^\circ\text{C}$ . It appears that vanadium in the PBN flux



SC5340.6SA

system stabilizes the rhombohedral structure over a much broader temperature range than is normally encountered for pure PBN. However, work on the pseudo-binary system  $BaV_2O_6$ -PBN:60 and  $Pb_{1-x}Ba_xV_2O_6$ -PBN:60 has resulted in the formation of the ferroelectric tetragonal PBN phase for one composition, and further research will be conducted on these systems based on these encouraging results.

Research has continued on the pseudo-binary morphotropic bronze systems  $Ba_2NaNb_5O_{15}$ - $Sr_2NaNb_5O_{15}$  (BNN-SNN) and  $Pb_2KNb_5O_{15}$ - $Ba_2NaNb_5O_{15}$  (PKN-BNN). Improved sintering of ceramic compositions from these systems has resulted in significantly improved dielectric properties, particularly near morphotropy. The system PKN-BNN shows particularly dramatic changes in dielectric properties near the morphotropic 0.75 PKN-0.25 BNN composition, with an abrupt discontinuity in the t and c lattice parameters, indicating the potential for particularly enhanced piezoelectric and electro-optic properties. Single crystal growth of selected compositions from these systems will be attempted in the coming period.



## 2.0 DEVELOPMENT OF OPTICAL QUALITY SBN:60

### 2.1 Materials Growth Techniques

Since most of the bronze compositions grown in our laboratory are based on solid solution systems, it is important that suitable growth techniques be developed to produce crystals free of optical defects such as striations, scattering centers and twinning. Striations and other defects are typical problems common to solid solution crystals, and it is often difficult to suppress them completely. However, these problems can effectively be reduced such that the crystals can be useful for optical device studies. This task is difficult; hence, the selection of appropriate growth techniques is critical in the present work. At present, three different techniques have been chosen to develop SBN and other bronze crystals. They are as follows:

1. Bulk Single Crystals: Czochralski technique
2. Thin Films: Liquid phase epitaxy (LPE)
3. Strip Crystals Edge defined film-fed technique

The first two techniques are well established in our current work, and bulk crystals and films of SBN compositions have already been grown. In the present report, the growth of striation-free SBN crystals and films is discussed with the associated growth problems.

### 2.2 Growth Procedure

$\text{Nb}_2\text{O}_5$ ,  $\text{SrCO}_3$ ,  $\text{Fe}_2\text{O}_3$ ,  $\text{CeO}_2$  and  $\text{BaCO}_3$  fine powders have been used as starting materials and weighed out in the desired proportions, as summarized in Table 1. The batch mixture is ball-milled in acetone for 20-30 h, and then poured into a large drying dish. The dried powder is placed in a platinum reaction dish and calcined at  $1000^\circ\text{C}$  for 10-15 h to eliminate carbonates and any possible carbon from the pyrolytic breakdown of residual acetone. The calcined powder is then ball-milled and refired in an oxygen flow of 2 cfh at



SC5340.6SA

1400°C for about 4-6 h. Phase checks and x-ray lattice constant measurements are made for each batch to ensure the use of a phase-pure bronze composition for crystal growth. A thick-walled platinum crucible of 2 x 2 in. in dimension is used for this growth, and this container holds roughly 450 g of melt composition.

Table 1  
Materials for Bulk Single Crystal SBN:60 Growth

| Crystal Composition       | Starting Materials                | Conditions and Remarks |  |
|---------------------------|-----------------------------------|------------------------|--|
| SBN:60                    | a. SrCO <sub>3</sub>              | 135.08 gms             | * Congruent melting composition                      |
|                           | b. BaCO <sub>3</sub>              | 115.48 gms             | * Large crystals can be grown                        |
|                           | c. Nb <sub>2</sub> O <sub>5</sub> | 398.73 gms             | * Large electro-optic coefficient ( $r_{33}$ )       |
|                           | Total Wt.                         | 649.26 gms             | * Melts at 1510°C                                    |
|                           | Growth Wt.                        | 450.00 gms             | * Crack-free and optical quality                     |
| SBN:60 + Fe <sup>3+</sup> | a. SrCO <sub>3</sub>              | 135.08 gms             | * Dielectric and electro-optic coefficient increased |
|                           | b. BaCO <sub>3</sub>              | 115.48 gms             | * Growth of large crystals is possible.              |
|                           | c. Nb <sub>2</sub> O <sub>5</sub> | 398.73 gms             | * Enhanced photorefractive properties                |
|                           | d. Fe <sub>2</sub> O <sub>3</sub> | 1.98 gms               | * Crack-free crystals                                |
|                           | Total Wt.                         | 651.24 gms             |  |
| SBN:60 + Ce <sup>3+</sup> | a. SrCO <sub>3</sub>              | 135.08 gms             | * Dielectric and electro-optic coefficient improved  |
|                           | b. BaCO <sub>3</sub>              | 115.48 gms             | * Growth of large crystals is possible               |
|                           | c. Nb <sub>2</sub> O <sub>5</sub> | 398.73 gms             | * Enhanced photorefractive properties                |
|                           | d. CeO <sub>2</sub>               | 1.00 gms               | * Crack-free and optical quality crystals            |
|                           | Total Wt.                         | 650.26 gms             |  |
| Growth Wt.                | 450.00 gms                        |                        |  |



### 2.3 Growth of Undoped SBN:60 Crystals

As summarized in Table 2, we have grown a number of undoped SBN:60 single crystals of excellent quality by the Czochralski technique. The quality of these crystals is generally excellent and the process appears to be highly reproducible for this composition. Since the ADC system is now well established to control the striation problem more effectively, we have begun to introduce a few more changes in the current system to improve the crystal quality further.

Recently, we found that small amounts of impurities have a drastic photorefractive effect in optical waveguide applications. Current optical measurements at NRL on SBN:60 crystals indicate that the elimination of impurities should significantly improve the optical quality for waveguide applications. In view of this, higher grade starting materials have been used in the present growth experiments (Table 3). Although minor changes in thermal gradients have occurred, this batch has been used to successfully grow two new SBN:60 crystals. The quality of these crystals is significantly better, and it is expected that by controlling the thermal gradients more effectively, it should be possible to further control the optical quality in these crystals. We expect that during the next six month period, we should have a sufficient number of crystals to analyze the crystal quality and thereby further refine the growth technique.

### 2.4 Growth of Doped SBN:60 Crystals

Since the optical quality and performance of SBN:60 crystals continues to be improved, it is important that other factors such as speed and sensitivity be enhanced for this family of crystals. Besides the further development of striation-free crystals, we have begun to examine the effects of



Table 2  
Growth of SBN Single Crystals

| To NRL | Boule No. | Date Grown | Boule Wt. gm | Boule Size, cm | Dip (°C) | Pull Rate, mm/hr | Rotation rpm | Remarks, Observations   |
|--------|-----------|------------|--------------|----------------|----------|------------------|--------------|---|
|        | 167*      | 11/1/83    | 20           | 1.2 x 3.0      | 1492     | ~ 9              | ~ 5          | Basal and vertical cracks, two deep twins, deep green color                                       |
|        | 168*      | 11/4/83    | 30           | 1.2 x 4.8      | 1492     | 9-10             | ~ 6          | Basal and vertical cracks, but no twins   |
|        | 169*      | 11/10/83   | 27           | 1.2 x 4.0      | 1492     | 8-10             | 5-6          | Uncracked upon cutting, green color, dopant distribution uneven                                   |
|        | 170*      | 1/6/84     | 6            | 1.0 x 1.8      | 1492     | 5-10             | 12-15        | Some twins and cracks, dark pink color, 1 1/4" x 1 1/4" crucible                                  |
|        | 171       | 1/18/84    | 4            | 0.5 x 4.5      | 1492     | 4-9              | 10           | Uncracked, pink color, good diameter control, striae closer together                              |
|        | 172       | 1/20/84    | ~ 6          | 0.6 x 5.0      | 1492     | 6-9              | 12-20        | Uncracked, pink color, diameter control by pull rate variation                                    |
|        | 173       | 1/31/84    | 21           | 1.2 x 5.0      | 1492     | 8-10             | 15-20        | New charge, good widening cone, some cracking upon seed removal                                   |
|        | 174       | 2/3/84     | 22           | 1.5 x 3.5      | 1491     | 4-10             | ~ 15         | Crack, defects from epi join  |
| *      | 175       | 2/7/84     | 25           | 1.4 x 3.0      | 1492     | ~ 6              | 15           | Uncracked, reversed seed dip end, good widening cone  |
|        | 176       | 2/9/84     | 31           | 1.5 x 3.0      | 1492     | ~ 6              | 8            | Uncracked, straight growth  |
| *      | 177       | 2/14/84    | 46           | 1.9 x 3.0      | 1490     | ~ 6              | 10           | Uncracked, minor coring down c-axis   |
|        | 178*      | 3/16/84    | 30           | 1.5 x 4.0      | 1490     | ~ 6              | 3-8          | Minor surface twinning, deep green color  |
|        | 179*      | 3/20/84    | 22           | 1.5 x 4.3      | 1488     | ~ 6              | 6-12         | Uncracked, coffee color   |
|        | 180       | 3/27/84    | 22           | 1.5 x 4.3      | 1488     | ~ 6              | ~ 8          | Uncracked, same color as 179, tendency to twin beyond 1.5 cm diameter                             |
|        | 181       | 4/4/84     | 44           | 1.9 x 2.6      | 1495     | ~ 6              | ~ 8          | Taken from furnace uncracked but cracks upon cutting  |
|        | 182       | 4/17/84    | 37           | 1.6 x 3.0      | 1492     | 5-8              | ~ 8          | Cracks upon seed removal, grew a bit off c-axis   |
|        | 183       | 5/8/84     | 26           | 1.4 x 3.0      | 1488     | 6-8              | ~ 6          | Uncracked, minor coring   |
|        | 184       | 5/15/84    | 37           | 1.7 x 3.0      | 1490     | 6-8              | ~ 6          | Seed section heavily defected (by etch pit observation) near edge. Removed uncracked from furnace |

Note 1: All crystals grown in O<sub>2</sub> flow of ~ 4 S.C.F.H.

Note 2: All crystals grown were of composition Sr/Ba of 0.61/0.39.

\* Doped SBN:60 single crystals.

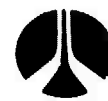


Table 3  
Impurities in Starting Chemicals used for SBN:60 Crystals  
(from Johnson Matthey Chemicals)

| Starting Chemical | Impurity | Previous Amount | Current Amount |
|-------------------|----------|-----------------|----------------|
| Nb2O5 *           | Ca       | ---             | 10 ppm         |
|                   | Mg       | ---             | > 1 ppm        |
|                   | Ta       | ---             | ---            |
| BaCO3             | Ca       | 1 ppm           | ---            |
|                   | Cu       | ~ 7 ppm         | ---            |
|                   | Mg       | > 1 ppm         | > 1 ppm        |
|                   | Na       | > 1 ppm         | > 1 ppm        |
|                   | Pb       | ---             | 3 ppm          |
| SrCO3             | Ri       | > 1 ppm         | 8 ppm          |
|                   | Ca       | > 1 ppm         | ---            |
|                   | Cu       | 1-10 ppm        | ---            |
|                   | Fe       | > 1 ppm         | > 1 ppm        |
|                   | Na       | > 1-2 ppm       | > 1 ppm        |
|                   | Mg       | > 1 ppm         | < 1 ppm        |
|                   | Pb       | ---             | 10 ppm         |

\* Basically, higher grade Nb2O5 has been used.

specific impurities in these crystals. Since the change in the refractive index for a ferroelectric crystal is given by

$$\Delta n = 1/3 n^3 r_{ij} E_{ij} \quad , \quad (2.1)$$

where  $r_{ij}$  = electro-optic coefficient and  $E_{ij}$  = space charge field, it is clear that both the electro-optic coefficient and space charge field should be increased to develop efficient material for photorefractive device applications. However, for a given crystal, e.g., SBN:60, the electro-optic coefficient is constant. Hence, it is important that the space charge field should be improved using proper dopants.



SC5340.6SA

Russian<sup>1</sup> and Japanese<sup>2</sup> researchers have demonstrated that the photorefractive sensitivity and response time of tungsten bronze SBN:60 ( $\text{Sr}_{0.6}\text{Ba}_{0.4}\text{Nb}_2\text{O}_5$ ) crystals can be effectively improved by introducing proper dopants. According to their work, Ce-doped SBN:60 crystals exhibit an exceptionally high photorefractive sensitivity of  $9.5 \times 10^{-3} \text{ cm}^2/\text{J}$ , a value that exceeds that of Fe-doped  $\text{LiNbO}_3$  ( $4 \times 10^{-5} \text{ cm}^2/\text{J}$ ) by more than two orders of magnitude. The response time for these crystals is marginal, but is substantially faster than for Fe-doped  $\text{LiNbO}_3$ . This work is significant and provides useful direction for future investigations in order to establish the factors controlling both sensitivity and speed. A summary of the proposed impurity ions and their possible valence states and site preference is given in Table 4.

Table 4  
Proposed Dopants for Photorefractive SBN  
SBN and Other Bronze Crystals

| Dopant     | Valence State  | Site Preference  |                  |                  |                                     |
|------------|--|------------------|------------------|------------------|-------------------------------------|
|            |  | 15-Fold          | 12-Fold          | 9-Fold           | 6-Fold                              |
| Cerium*    | $\text{Ce}^{3+}$ , $\text{Ce}^{4+}$                    | $\text{Ce}^{3+}$ | $\text{Ce}^{3+}$ | $\text{Ce}^{4+}$ | $\text{Ce}^{4+}$                    |
| Terbium    | $\text{Tb}^{3+}$ , $\text{Tb}^{4+}$                    | --               | $\text{Tb}^{3+}$ | $\text{Tb}^{4+}$ | $\text{Tb}^{4+}$                    |
| Iron*      | $\text{Fe}^{3+}$ , $\text{Fe}^{2+}$                    | --               | --               | $\text{Fe}^{2+}$ | $\text{Fe}^{2+}$ , $\text{Fe}^{3+}$ |
| Manganese  | $\text{Mn}^{2+}$ , $\text{Mn}^{3+}$ , $\text{Mn}^{4+}$ | --               | --               | $\text{Mn}^{2+}$ | $\text{Mn}^{2+}$ , $\text{Mn}^{3+}$ |
| Titanium   | $\text{Ti}^{4+}$ , $\text{Ti}^{3+}$                    | --               | --               | --               | $\text{Ti}^{4+}$ , $\text{Ti}^{3+}$ |
| Molybdenum | $\text{Mo}^{5+}$ , $\text{Mo}^{4+}$                    | --               | --               | --               | $\text{Mo}^{6+}$ , $\text{Mo}^{4+}$ |
| Niobium    | $\text{Nb}^{5+}$ , $\text{Nb}^{4+}$                    | --               | --               | --               | $\text{Nb}^{5+}$ , $\text{Nb}^{4+}$ |

\* Used as  $\text{CeO}_2$  and  $\text{Fe}_2\text{O}_3$



SC5340.6SA

Table 5 summarizes the crystal compositions, dopants used and growth conditions examined thus far. Both Fe and Ce-doped SBN:60 single crystals have been grown by the Czochralski technique under identical conditions used for undoped SBN:60 crystals. In this material  $Fe^{3+}$  prefers the 6-fold coordinate sites, while the  $Ce^{3+}$  is expected to occupy either 12- or 9-fold coordinated sites in the structure. Both Russian and Japanese reserachers have used Ce in this crystal, but from their work, the valance state of Ce and its site preference are not clear.<sup>2</sup>

Table 5  
Growth Data on Doped and Undoped SBN:60 Crystals

| Property                   | SBN:60                | SBN:60 + $Fe^{3+}$                | SBN:60 + $Ce^{4+}$    |
|----------------------------|-----------------------|-----------------------------------|-----------------------|
| Symmetry                   | 4 mm                  | 4 mm                              | 4 mm                  |
| Color of Crystal           | Pale cream            | Green<br>Yellow (O <sub>2</sub> ) | Pink                  |
| Conc. of Dopants           | ---                   | ~ 1.0 mol%                        | ~ 0.1 mol%            |
| Curie Temperature (°C)     | 72                    | 51                                | 70                    |
| Dielectric Constant (23°C) | $\epsilon_{33} = 600$ | $\epsilon_{33} = 3400$            | $\epsilon_{33} = 940$ |
| Quality                    | Excellent             | Good                              | Excellent             |
| Photorefractive Response   | Good                  | Better                            | Excellent             |
| Size (diameter)            | 2-3 cm                | ~ 1.5 cm                          | 1.0 cm                |

Growth of these doped crystals has been successful, and crystals as large as 1 cm to 1.5 cm in diameter have been grown. The addition of the 3-d ( $Fe^{3+}$ ) and 4-f ( $Ce^{3+}$ ) cations in SBN:60 increases the thermal conductivity of the material; hence, necessary changes in the after-heater must be made to control thermal conditions in the crucible and near the solid-liquid interface. Since the concentrations of these dopants is relatively low, these changes are minor; however, it is important in the present work to further evaluate these conditions in order to develop optical quality crystals.



The Fe-doped SBN:60 crystals are deep green in color; however, this color changes to a deep yellow after annealing in an oxygen atmosphere at 1000°C. This result indicates that at elevated temperatures  $Nb^{5+}$  reduces to  $Nb^{4+}$ , which is again a transition metal ion and contributes to the color of the crystal. The Ce-doped SBN:60 crystals show a pink color which persists after oxidation at 1000°C.

Fracture-free and reasonably good quality crystals have been grown. Although the growth of bigger sized crystals is possible in the present set-up, the technique at present will be confined to smaller size crystals. Figure 1 shows typical Ce-doped SBN:60 single crystals grown along the c-axis. Once the initial electro-optic and photorefractive properties of these doped crystals are established, plans will be made to improve their size and quality. X-ray diffraction studies show that crystal habit for these doped crystals is similar to undoped crystals, and is based on 24 facets of four prisms: (110), (120), (100) and (130).

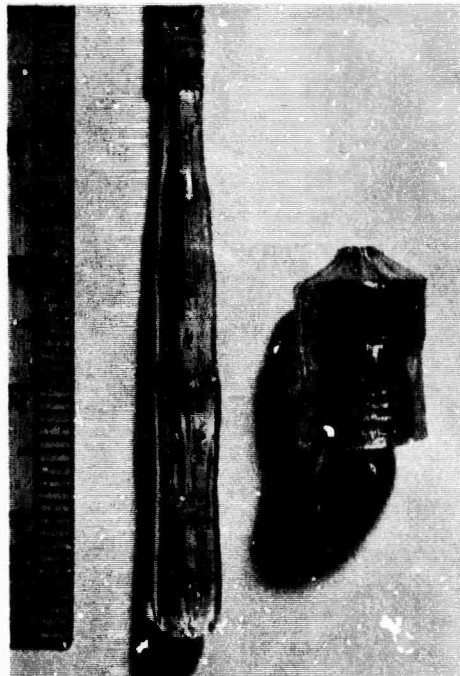


Fig. 1 Ce-doped SBN:60 crystals grown by the Czochralski method.



SC5340.6SA

Optical evaluation of doped SBN:60 crystals indicates the presence of weak striations which are basically connected to the addition of  $\text{Fe}^{3+}$  and  $\text{Ce}^{3+}$  cations. It is believed that these striations can be suppressed or partially removed by controlling the thermal gradients in the crucible and near the solid-liquid interface. This task will be undertaken only when the dopant concentration is optimized. As shown in Table 5, the addition of  $\text{Fe}^{3+}$  and  $\text{Ce}^{3+}$  cations has significantly enhanced the dielectric constant, which indicates an increase in the electro-optic coefficient ( $r_{33}$ ) in similar proportions. It was also found that the photorefractive sensitivity was substantially increased with dopants. These results are discussed in Section 6.0.

Based on all of these observations, we expect that by optimally controlling dopant concentrations in SBN:60 crystals, it should be possible to effectively investigate both photorefractive sensitivity and speed. During the next six months, the following experiments will be tried for photorefractive applications. They are as follows:

- Establish valence states of Fe and Ce cations in SBN:60 crystals.
- Establish optimum concentrations of Fe and Ce necessary for increased photorefractive sensitivity and speed.
- Establish the dielectric and electro-optic properties for these doped crystals and their effects on photorefractive properties.
- Develop more SBN:60 crystals with varying dopant concentrations.



### 3.0 LIQUID PHASE EPITAXIAL GROWTH OF BRONZE COMPOSITIONS

Large tungsten bronze single crystals are often very difficult to grow by the Czochralski method, particularly in the case of incongruently melting compositions (e.g., SBN:75) and compositions with volatile constituent ions (e.g.,  $Pb^{2+}$  in  $Pb_{1-x}Ba_xNb_2O_6$ ). In such cases, an alternative growth method is the liquid phase epitaxy (LPE) technique, which can be used to develop optical quality tungsten bronze thin films using existing bronze single crystal substrate. This technique is important not only for thin film fabrication for electro-optic, nonlinear optic and piezoelectric device applications, but also in the development of new bronze compositions for property evaluation.

The present work has focused on the development of LPE films of the tetragonal bronze compositions SBN:75 and PBN:60. Since large single crystals of SBN:50 and SBN:60 are available for use as substrate material with minimal lattice mismatch to the LPE bronze compositions, we do not anticipate any major problems in actual film growth. However, successful film growth of these selected compositions is inherently dependent on the thermodynamics of the flux systems used, with the three major requirements being (1) a sufficiently low melt temperature, (2) the absence of second phases, and (3) the maintenance of the desired bronze composition in the as-grown film. The results of our current work are discussed in the following section.

#### 3.1 Flux Systems for SBN:75

As discussed in a previous report, we have successfully demonstrated the LPE growth of SBN:60 thin films on SBN:60 substrate using a  $BaV_2O_6$ - $Sr_{0.5}Ba_{0.5}Nb_2O_6$  flux system. However, in the case of SBN:75 thin film growth, a composition which displays the highest electro-optic and piezoelectric coefficients in the SBN family, we did not know the proper flux recipe required in order to maintain compositional control over the as-grown film. Therefore, the present work has focused on the quaternary phase diagram for the SrO-BaO-



$\text{Nb}_2\text{O}_5$ - $\text{V}_2\text{O}_5$  system in order to understand its thermodynamic behavior. Because of the extensive work required to build the entire quaternary phase diagram, our work has been restricted to possible bronze-forming flux systems such as  $\text{BaV}_2\text{O}_6$ - $\text{Sr}_{0.5}\text{Ba}_{0.5}\text{Nb}_2\text{O}_6$ ,  $\text{SrV}_2\text{O}_6$ - $\text{Sr}_{0.5}\text{Ba}_{0.5}\text{Nb}_2\text{O}_6$ , and (.65)  $\text{Sr}_{1-x}\text{Ba}_x\text{Nb}_2\text{O}_6$ -(.35) $\text{Sr}_{0.5}\text{Ba}_{0.5}\text{Nb}_2\text{O}_6$ . The ranges covered in the quaternary phase diagram with these systems are shown in Fig. 2.

A variety of flux compositions were prepared and then sintered or melted at either  $1000^\circ\text{C}$  or  $1250^\circ\text{C}$ . After leaching away the remaining vanadates with a dilute nitric acid solution, the structures of the remaining niobate solids were identified using powder x-ray diffraction measurements and analysis. The results of this work are presented in Table 6.

SC84-26697

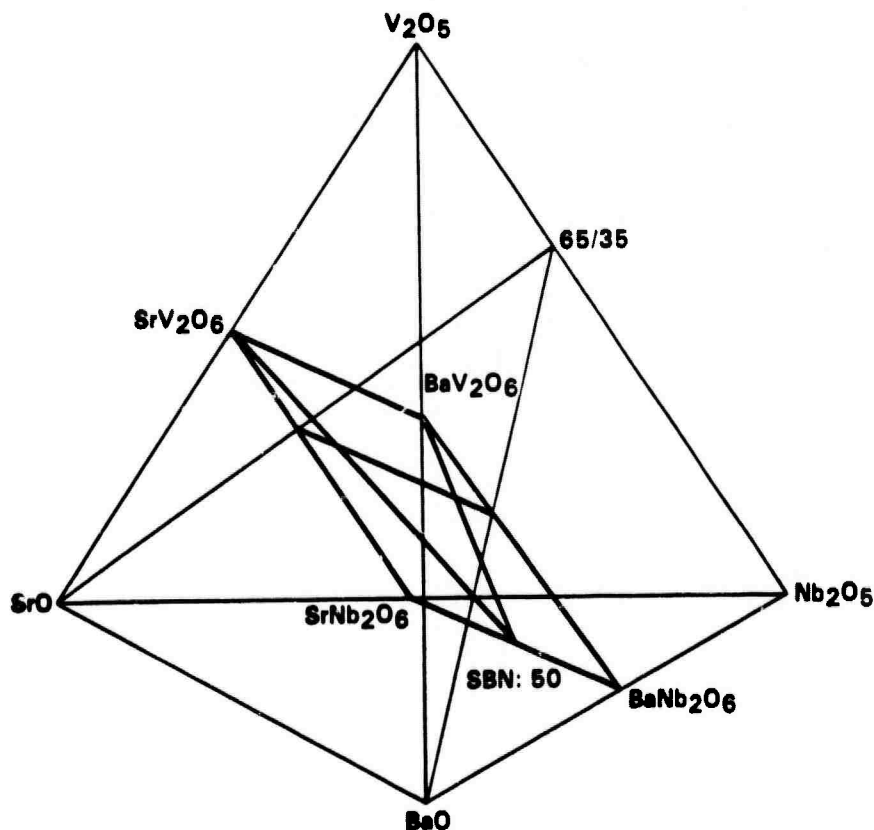


Fig. 2 Quaternary phase diagram of the  $\text{SrO}$ - $\text{BaO}$ - $\text{Nb}_2\text{O}_5$  system.



Table 6  
LPE Fluxes for SBN

| No. | Composition  | Sr/Sr + Ba | Temperature (°C) | Remaining Phase                        |
|-----|--|------------|------------------|--|
| 1   | 65% SrV <sub>2</sub> O <sub>6</sub> + 35% Sr <sub>0.5</sub> Ra <sub>0.5</sub> Nb <sub>2</sub> O <sub>6</sub>                                   | 0.825      | Melted 1000      | SrNb <sub>2</sub> O <sub>6</sub>       |
| 2   | 65% Sr <sub>0.5</sub> Ra <sub>0.5</sub> V <sub>2</sub> O <sub>6</sub> + 35% Sr <sub>0.5</sub> Ra <sub>0.5</sub> Nb <sub>2</sub> O <sub>6</sub> | 0.50       | Melted 1000      | Other                                  |
| 3   | 65% Sr <sub>0.3</sub> Ra <sub>0.7</sub> V <sub>2</sub> O <sub>6</sub> + 35% Sr <sub>0.5</sub> Ra <sub>0.5</sub> Nb <sub>2</sub> O <sub>6</sub> | 0.36       | Melted 1000      | Other                                  |
| 4   | 65% Sr <sub>0.5</sub> Ra <sub>0.8</sub> V <sub>2</sub> O <sub>6</sub> + 35% Sr <sub>0.5</sub> Ra <sub>0.5</sub> Nb <sub>2</sub> O <sub>6</sub> | 0.305      | Melted 1000      | Other                                  |
| 5   | 65% Sr <sub>0.1</sub> Ra <sub>0.9</sub> V <sub>2</sub> O <sub>6</sub> + 35% Sr <sub>0.5</sub> Ra <sub>0.5</sub> Nb <sub>2</sub> O <sub>6</sub> | 0.24       | Melted 1000      | SBN:37                                 |
| 6   | 65% BaV <sub>2</sub> O <sub>6</sub> + 35% Sr <sub>0.5</sub> Ra <sub>0.5</sub> Nb <sub>2</sub> O <sub>6</sub>                                   | 0.175      | Melted 1000      | SBN:37                                 |
| 7   | 40% SrV <sub>2</sub> O <sub>6</sub> + 60% Sr <sub>0.5</sub> Ra <sub>0.5</sub> Nb <sub>2</sub> O <sub>6</sub>                                   | 0.70       | Melted 1250      | SrNb <sub>2</sub> O <sub>6</sub>       |
| 8   | 30% SrV <sub>2</sub> O <sub>6</sub> + 70% Sr <sub>0.5</sub> Ra <sub>0.5</sub> Nb <sub>2</sub> O <sub>6</sub>                                   | 0.65       | Sintered 1250    | SBN + SrNb <sub>2</sub> O <sub>6</sub> |
| 9   | 20% SrV <sub>2</sub> O <sub>6</sub> + 70% Sr <sub>0.5</sub> Ra <sub>0.5</sub> Nb <sub>2</sub> O <sub>6</sub>                                   | 0.65       | Sintered 1250    | SBN:58                                 |
| 10  | 40% BaV <sub>2</sub> O <sub>6</sub> + 60% Sr <sub>0.5</sub> Ra <sub>0.5</sub> Nb <sub>2</sub> O <sub>6</sub>                                   | 0.30       | Melted 1250      | SBN:X                                  |
| 11  | 50% Sr <sub>0.5</sub> Ra <sub>0.5</sub> V <sub>2</sub> O <sub>6</sub> + 50% Sr <sub>0.5</sub> Ra <sub>0.5</sub> Nb <sub>2</sub> O <sub>6</sub> | 0.50       | Sintered 1250    | SrNb <sub>2</sub> O <sub>6</sub>       |

SC5340.6SA

Figure 3 shows the phase diagram for the system  $\text{SrV}_2\text{O}_6\text{-BaV}_2\text{O}_6\text{-SrNb}_2\text{O}_6\text{-BaNb}_2\text{O}_6$ , which is the smaller quaternary region examined here in the larger  $\text{SrO-BaO-Nb}_2\text{O}_5\text{-V}_2\text{O}_5$  phase diagram of Fig. 2. The solid circles in Fig. 3 represent tetragonal tungsten bronze SBN phases, and the squares represent other observed phases according to the results listed in Table 6. From this work, it is seen that only in the shaded region of Fig. 3, which includes the flux compositions No. 5, 6, 9 and 10, can single phase bronze compositions be found. The range of this bronze forming region for  $\text{Sr}_{1-x}\text{Ba}_x\text{Nb}_2\text{O}_6$  is  $0.25 < x < 0.75$ , as shown in Fig. 3.

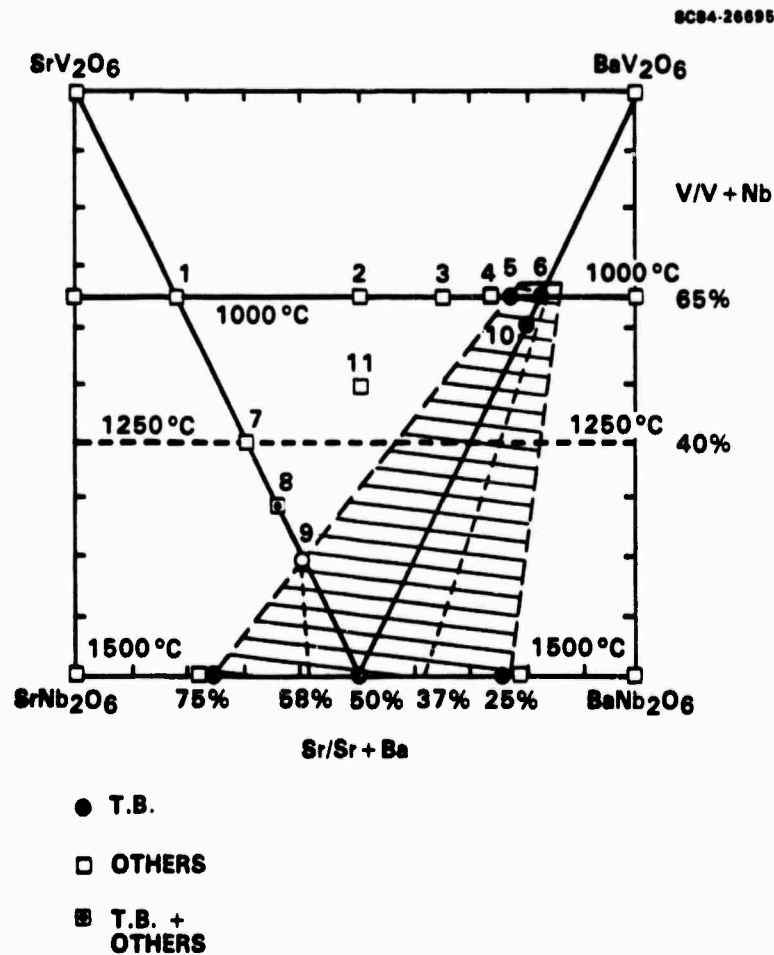


Fig. 3 Quaternary phase diagram of the  $\text{SrV}_2\text{O}_6\text{-BaV}_2\text{O}_6\text{-SrNb}_2\text{O}_6\text{-BaNb}_2\text{O}_6$  system.



SC5340.6SA

At the present time, there is some uncertainty in the determination of the actual SBN compositions formed in this region. However, since we were able to establish that SBN:37 was grown from flux No. 6 and SBN:58 from flux No. 9, two tie-lines can be drawn from these flux points in the phase diagram shown in Fig. 3 (dashed lines). Hence, in order to grow LPE films with the composition  $\text{Sr}_{0.75}\text{Ba}_{0.25}\text{Nb}_2\text{O}_6$ , we must work in the very small region of flux compositions bounded by the SBN:58 tie-line.

Considering the melting points for various flux compositions, e.g., roughly  $1000^\circ\text{C}$  for  $V/(V+\text{Nb}) = 0.65$ ,  $1250^\circ\text{C}$  for  $V/(V+\text{Nb}) = 0.40$  and  $1500^\circ\text{C}$  for  $V/(V+\text{Nb}) = 0$ , it is clear that the LPE growth of the SBN:75 bronze composition from the  $\text{SrO}-\text{BaO}-\text{Nb}_2\text{O}_5-\text{V}_2\text{O}_5$  flux system may not be particularly easy. Not only must one deal with a relatively narrow range of suitable flux compositions, but also a necessarily high flux melting point greater than  $1350^\circ\text{C}$ .

### 3.2 Flux Systems for PBN:60

As discussed previously, a  $\text{V}_2\text{O}_5$  solvent has been initially selected for the growth of tetragonal  $\text{Pb}_{0.6}\text{Ba}_{0.4}\text{Nb}_2\text{O}_6$  thin films on SBN:60 substrates. Several possible bronze-forming flux systems have been studied during the past several months, including  $\text{Pb}_2\text{V}_2\text{O}_7-\text{Pb}_{0.6}\text{Ba}_{0.4}\text{Nb}_2\text{O}_6$ ,  $\text{BaV}_2\text{O}_6-\text{Pb}_{0.6}\text{Ba}_{0.4}\text{Nb}_2\text{O}_6$  and  $\text{Pb}_{2-x}\text{Ba}_x\text{V}_2\text{O}_7-\text{Pb}_{0.6}\text{Ba}_{0.4}\text{Nb}_2\text{O}_6$ . Preparation and evaluation procedures were essentially the same as those for the SBN flux systems, with dilute nitric acid being used to leach out any vanadates prior to powder x-ray diffraction measurements. A summary of the fluxes examined is given in Table 7.

Figure 4 shows the phase diagram of the  $\text{Pb}_2\text{V}_2\text{O}_7-\text{Ba}_2\text{V}_2\text{O}_7-\text{PbNb}_2\text{O}_6-\text{BaNb}_2\text{O}_6$  system in which the solid circles represent the ferroelectric tetragonal PBN phase, triangles represent the nonferroelectric rhombohedral phase, and squares represent the presence of other second phases. The shadowed area of Fig. 4, which includes flux systems No. 1, 2 and 5 in Table 7, is the rhombohedral phase formation region for PBN. No orthorhombic phase was ever found in this region, even when material was quenched to room temperature from  $1250^\circ\text{C}$ .



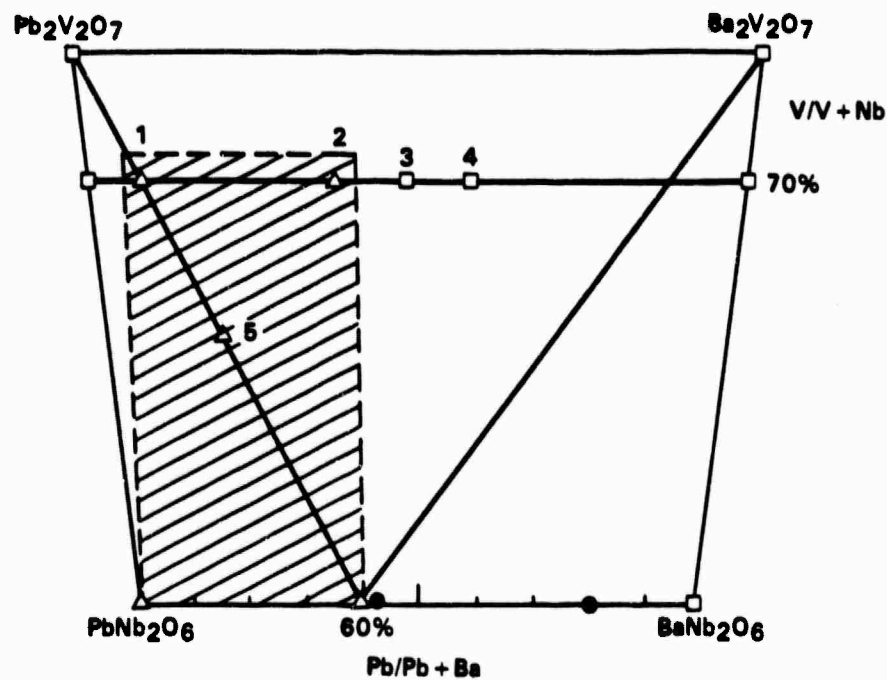
Table 7  
LPE Fluxes for PRN

| No. | Composition  | Pb/Pb + Ra | Melting Temp.<br>(°C) | Remaining Phase                             |
|-----|--|------------|-----------------------|---|
| 1   | 70% Pb <sub>2</sub> V <sub>2</sub> O <sub>7</sub> + 30% Pb <sub>0.6</sub> Ra <sub>0.4</sub> Nb <sub>2</sub> O <sub>6</sub>                     | 0.93       | Melted, 1000 and 1250 | Rhomb. PRN                                  |
| 2   | 70% Pb <sub>1.2</sub> Ba <sub>0.8</sub> V <sub>2</sub> O <sub>7</sub> + 30% Pb <sub>0.6</sub> Ra <sub>0.4</sub> Nb <sub>2</sub> O <sub>6</sub> | 0.60       | Melted, 1000 and 1250 | Rhomb. PRN                                  |
| 3   | 70% Pb <sub>0.8</sub> Ba <sub>1.2</sub> V <sub>2</sub> O <sub>7</sub> + 30% Pb <sub>0.6</sub> Ra <sub>0.4</sub> Nb <sub>2</sub> O <sub>6</sub> | 0.50       | Melted, 1000          | Other                                       |
| 4   | 60% Pb <sub>0.6</sub> Ra <sub>1.4</sub> V <sub>2</sub> O <sub>7</sub> + 30% Pb <sub>0.6</sub> Ra <sub>0.4</sub> Nb <sub>2</sub> O <sub>6</sub> | 0.43       | Melted, 1000          | Other                                       |
| 5   | 50% Pb <sub>2</sub> V <sub>2</sub> O <sub>7</sub> + 50% Pb <sub>0.6</sub> Ra <sub>0.4</sub> Nb <sub>2</sub> O <sub>6</sub>                     | 0.87       | Melted, 1250          | Rhomb. PRN                                  |
| 6   | 80% BaV <sub>2</sub> O <sub>6</sub> + 20% Pb <sub>0.6</sub> Ra <sub>0.4</sub> Nb <sub>2</sub> O <sub>6</sub>                                   | 1.12       | Melted, 1000          | Other                                       |
| 7   | 70% BaV <sub>2</sub> O <sub>6</sub> + 30% Pb <sub>0.6</sub> Ra <sub>0.4</sub> Nb <sub>2</sub> O <sub>6</sub>                                   | 0.18       | Melted, 1000          | Tet. PRN + RaNb <sub>2</sub> O <sub>6</sub> |
| 8   | 50% RaV <sub>2</sub> O <sub>6</sub> + 50% Pb <sub>0.6</sub> Ra <sub>0.4</sub> Nb <sub>2</sub> O <sub>6</sub>                                   | 0.30       | Melted, 1250          | Tet. PRN                                    |



SC5340.6SA

SC04-26884



- TET PBN
- ▲ RHOM PBN
- OTHERS

Fig. 4 Quaternary phase diagram of the  $Pb_2V_2O_7$ - $Ba_2V_2O_7$ - $PbNb_2O_6$ - $BaNb_2O_6$  system.

This result is to be compared with that for normal  $Pb_{1-x}Ba_xNb_2O_6$ ,  $x < 0.6$ , in which the orthorhombic phase forms when the material is quenched from 1250°C and the rhombohedral phase forms when quenched from 1000°C. It appears, then, that the presence of vanadium in the PBN flux system stabilizes the rhombohedral structure over a much broader temperature range than is normally encountered for PBN.

Since we were unable to find either tetragonal or orthorhombic bronze phases for the  $Pb_2V_2O_7$ - $Pb_{0.6}Ba_{0.4}Nb_2O_6$  and  $Pb_{2-x}Ba_xV_2O_7$ - $Pb_{0.6}Ba_{0.4}Nb_2O_6$  flux systems, we then turned our attention to the systems  $BaV_2O_6$ - $Pb_{0.6}Ba_{0.4}Nb_2O_6$  and  $Pb_{1-x}Ba_xV_2O_6$ - $Pb_{0.6}Ba_{0.4}Nb_2O_6$ , as shown in the phase diagram in Fig. 5. Initial results in this flux system look very promising, as a ferroelectric



SC5340.6SA

tetragonal PRN phase was found for flux No. 8 of Table 7, indicated by the solid circle in Fig. 5. Based on these encouraging results, future work will focus on the following:

1. Development of the  $\text{BaV}_2\text{O}_6\text{-Pb}_{0.6}\text{Ba}_{0.4}\text{Nb}_2\text{O}_6$  flux system.
2. Development of the  $\text{Pb}_{1-x}\text{Ba}_x\text{V}_2\text{O}_6\text{-Pb}_{0.6}\text{Ba}_{0.4}\text{Nb}_2\text{O}_6$  flux system.
3. Lattice parameter standards for  $\text{Pb}_{1-x}\text{Ba}_x\text{Nb}_2\text{O}_6$  for comparison with flux-growth phases.

With successful development of suitable PRN compositions from these flux systems,  $\text{Pb}_{1-x}\text{Ba}_x\text{Nb}_2\text{O}_6$  thin films will then be grown on SBN:60 substrates using the LPE technique.

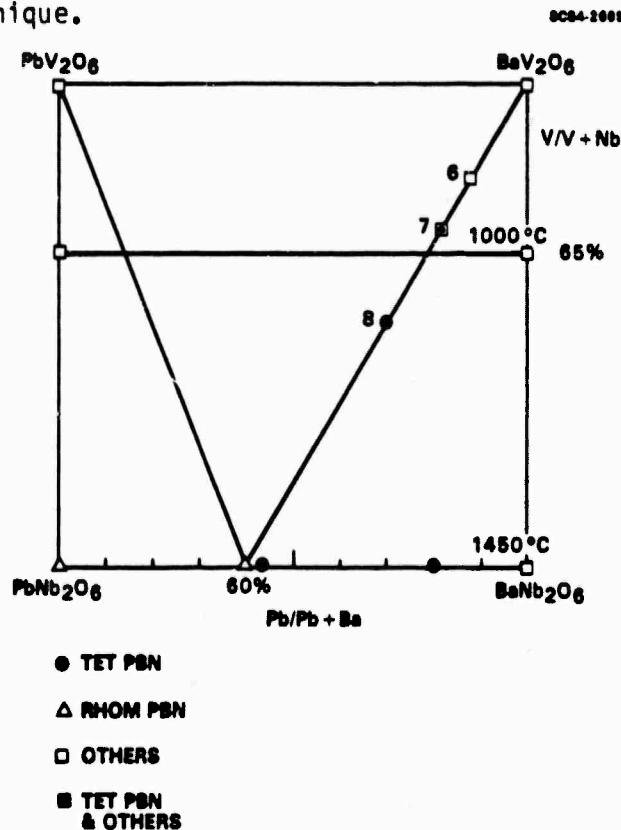


Fig. 5 Phase diagram of the  $\text{PbV}_2\text{O}_6\text{-BaV}_2\text{O}_6/\text{PbNb}_2\text{O}_6\text{-BaNb}_2\text{O}_6$  system.



#### 4.0 NEW TUNGSTEN BRONZE SYSTEMS FOR ELECTRO-OPTIC STUDIES

Several of the more interesting tungsten bronze systems show morphotropic phase boundaries (MPB) which depend primarily on composition rather than on temperature. Ceramic or single crystal compositions adjacent to such boundaries show considerable enhancement of electro-optic, dielectric, piezoelectric, electromechanical and pyroelectric properties because of the proximity in energy of an alternate ferroelectric structure. In the present work, two such systems,  $Ba_2NaNb_5O_{15}$ - $Sr_2NaNb_5O_{15}$  and  $Pb_2KNb_5O_{15}$ - $Ba_2NaNb_5O_{15}$ , have been investigated and are found to have MPB conditions with exceptionally high dielectric and other properties. In this report, we present further data on these bronze systems based on work during the past six months.

##### 4.1 $Ba_2NaNb_5O_{15}$ - $Sr_2NaNb_5O_{15}$ System

Tungsten bronze barium sodium niobate (BNN) has been shown to be an outstanding material for electro-optic and nonlinear optic applications, particularly for second harmonic generation of near-IR laser radiation. The material was first discovered in 1967 by researchers at Bell Labs,<sup>3</sup> and was found to have a number of useful nonlinear optic and piezoelectric properties. Stoichiometric  $Ba_2NaNb_5O_{15}$  is orthorhombic at room temperature with lattice constants  $a = 17.592\text{\AA}$ ,  $b = 17.626\text{\AA}$  and  $c = 3.995\text{\AA}$ , as determined from high angle x-ray measurements.<sup>4</sup> Above  $260^\circ\text{C}$ , an orthorhombic to tetragonal transformation occurs in which microtwinning is usually observed in single crystals, but with no significant dielectric anomalies. The Curie point is at approximately  $570^\circ\text{C}$ .

Based on our earlier theoretical work on the tungsten bronze family<sup>5</sup> and experimental work on  $Pb_{1-x}Ba_xNb_2O_6$ , an enhancement of the piezoelectric, pyroelectric and electro-optic properties can be anticipated for tungsten bronze compositions which exhibit a morphotropic boundary condition between the tetragonal and orthorhombic phases. To this end, we began an investigation of the pseudo binary system  $(1-x)Ba_2NaNb_5O_{15}$ - $(x)Sr_2NaNb_5O_{15}$  during the



SC5340.6SA

previous reporting period. In the present report, we present further refinements of this work.

The materials used for each particular composition were prepared by the normal procedure of mixing, calcining at 950°C, and then ball-milling for 12-18 h. The cold-pressed disks were then sintered for 2 h at 1280-1380°C, depending on composition. It was found during earlier work that many of the compositions were not well sintered and, hence, a considerable effort was made to determine the optimum sintering conditions. In particular, it was found that much higher sintering temperatures are required for BNN-rich compositions, with an optimum sintering temperature of 1380°C for pure  $\text{Ba}_2\text{NaNb}_5\text{O}_{15}$ . The resulting dielectric properties are considerably greater at the Curie point  $T_C$ , and the characteristics as a function of temperature are substantially sharpened near  $T_C$ . The variation in the Curie point as a function of composition is shown in Fig. 6, with the characteristic sharp drop in  $T_C$  occurring at the morphotropic (0.40)BNN-(0.60)SNN composition.

Figure 7 shows the dielectric properties as a function of composition. The major enhancement over the previously reported data is an increase in the dielectric properties at  $T_C$  for BNN-rich compositions as a result of improved ceramic sintering. The dielectric constant at the Curie point is essentially flat on either side of the morphotropic boundary, with an abrupt factor of two jump in the dielectric constant at the MPB. The dielectric properties at room temperature are generally monotonic with composition, rising from a value of  $\epsilon = 100$  for BNN to nearly 2000 for SNN. However, an anomalously high value of  $\epsilon = 1200$  occurred for  $x = 0.67$ ; it is not presently clear if this is a true local maximum near the morphotropic phase boundary or if the SNN-rich compositions are still inadequately sintered. The steep rise in the room temperature dielectric constant for  $x > 0.8$  is due to the onset of a second transition peak which occurs below room temperature. The influence of this second transition can be seen in the dielectric properties for  $\text{Sr}_2\text{NaNb}_5\text{O}_{15}$  (SNN) shown in Fig. 8; preliminary low temperature measurements show this to be a very broad dielectric peak with a maximum near -50°C.



SC5340.6SA

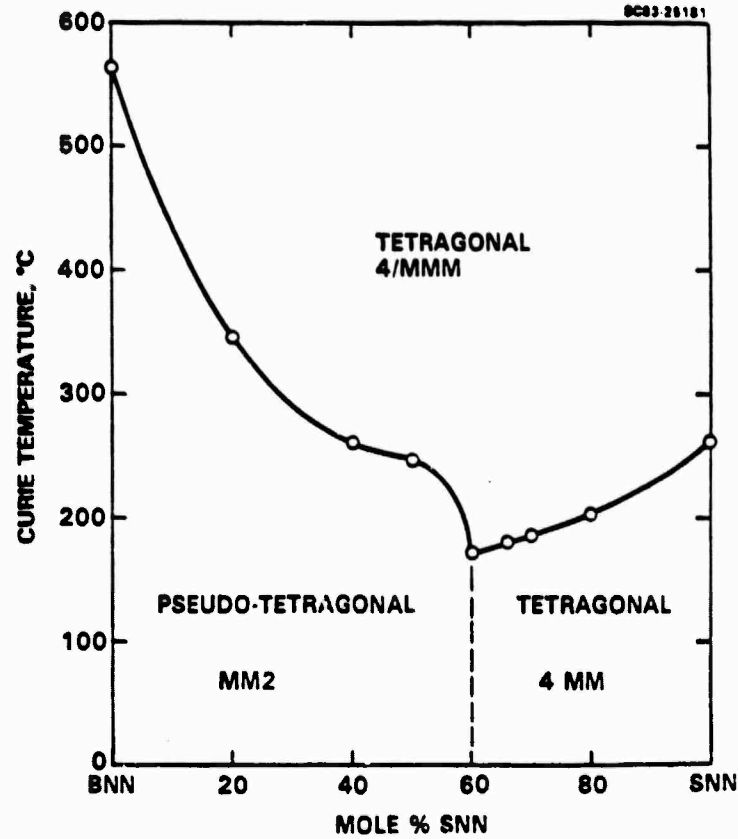


Fig. 6 Morphotropic phase boundary conditions for the system BNN-SNN.

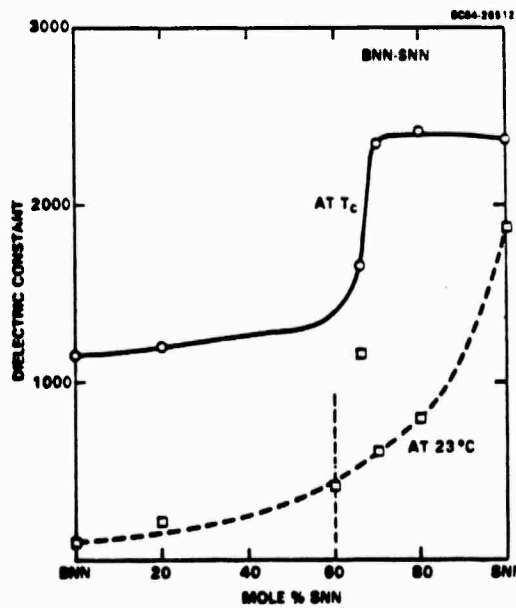


Fig. 7 Dielectric constant (at 10 kHz) vs composition for the system BNN-SNN.

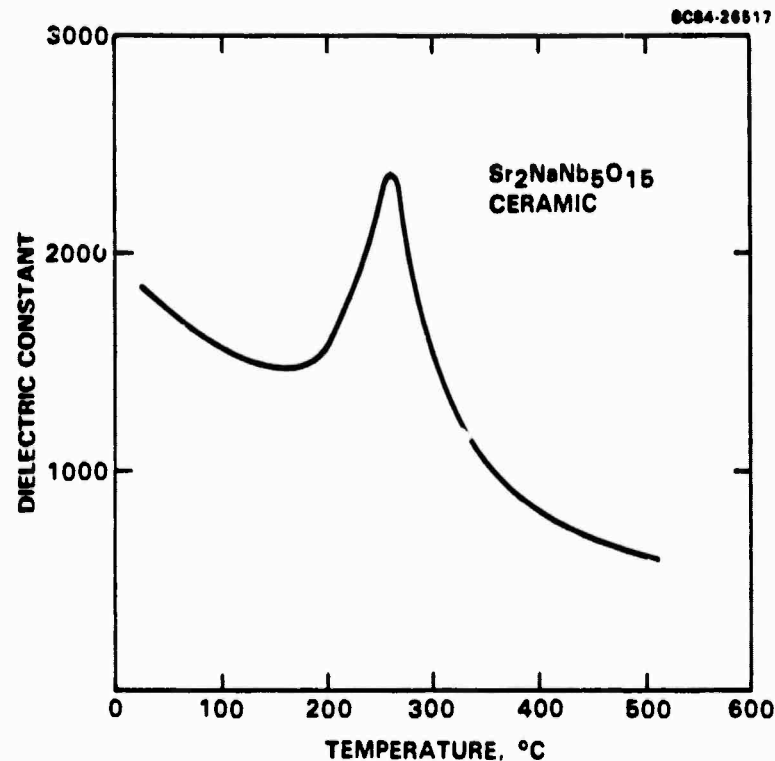


Fig. 8 Dielectric constant of ceramic  $\text{Sr}_2\text{NaNb}_5\text{O}_{15}$  (SNN) as a function of temperature.

We have performed hot-pressed ceramic densification on two compositions in the region of the morphotropic phase boundary for this system, specifically 0.40 BNN-0.60 SNN and 0.30 BNN-0.70 SNN. In both cases, the material was hot-pressed at 4000 psi for 2 h at 1280°C, and then cooled slowly to room temperature. Because of the nitrogen ambient atmosphere required by the graphite dies for this press, the reduced samples were oxidized for 12 h at 1070°C subsequent to densification. The resulting ceramics were crack-free and a uniform off-white in color. The dielectric properties for these densified ceramic compositions are summarized in Table 8 for measurements taken parallel and perpendicular to the uniaxial pressing direction. It is interesting to note that the measured dielectric values are comparable to those measured for normally sintered ceramic material. The most significant anisotropy appears



SC5340.6SA

for the 0.30 BNN-0.70 SNN composition, indicating partial grain orientation. This result is not unexpected, since in the morphotropic 0.40 BNN-0.60 SNN composition possesses both orthorhombic (pseudo-tetragonal) and tetragonal phases and, hence, is less inclined to demonstrate a preferential grain orientation.

Table 8  
Dielectric Properties of Hot-Pressed BNN-SNN

| Composition       | Dielectric Constant*<br>Cut | @ T <sub>c</sub> |                  | T <sub>c</sub> (°C) |
|-------------------|-----------------------------|------------------|------------------|---------------------|
|                   |                             | @ 23°C           | @ T <sub>c</sub> |                     |
| 0.30 BNN-0.70 SNN | Para.                       | 835              | 2250             | 216                 |
|                   | Perp.                       | 925              | 3140             |                     |
| 0.40 BNN-0.60 SNN | Para.                       | 800              | 2560             | 221                 |
|                   | Perp.                       | 800              | 3230             |                     |

\* at 10 kHz



#### 4.2 Pb<sub>2</sub>KNb<sub>5</sub>O<sub>15</sub>-Ba<sub>2</sub>NaNb<sub>5</sub>O<sub>15</sub> System

Another tungsten bronze of interest is Pb<sub>2</sub>KNb<sub>5</sub>O<sub>15</sub> (PKN). This composition has been successfully grown in hot-pressed dense ceramic form by Nagata et al<sup>6</sup> in Japan with a high electrochemical coupling constant,  $k_t = 0.40$ , and good polarization. As such, it represents an attractive candidate for SAW, piezoelectric and pyroelectric device applications. However, its relatively high Curie point (470°C) makes it very difficult to completely pole. It is also prone to cracking above 1200°C growth temperatures<sup>6</sup> and, hence, the attainment of optically transparent hot-pressed material remains unlikely.

Because of the orthorhombic structure of PKN, the possibility presented itself of obtaining a morphotropic phase composition in combination with pseudo tetragonal BNN. To this end, we began an investigation of the pseudo binary bronze system (1-x)Pb<sub>2</sub>KNb<sub>5</sub>O<sub>15</sub>-(x)Ba<sub>2</sub>NaNb<sub>5</sub>O<sub>15</sub> using cold-pressed and sintered ceramic samples. A morphotropic phase boundary condition was, indeed, found for the composition 0.75 PKN-0.25 BNN with a sharp minimum in  $T_c$  of 270°C. However, cracking was a major problem in these ceramics, even after lowering the sintering temperature for PKN-rich samples; hence, much of the dielectric data were not viewed with confidence.

The addition of excess PbO, on the order of 1-3%, has been found to dramatically improve the quality of ceramics prepared from this system with the total disappearance of microcracks. Measured weight losses show the ceramics to be approximately 1-2% Pb<sup>2+</sup>-deficient after sintering for 4 h. Measurements of the Curie transition temperature as a function of composition for (1-x)PKN-(x)BNN are shown in Fig. 9, and are only slightly different from earlier data. However, measured values for the dielectric constant at  $T_c$  and at room temperature now show much steeper characteristics at the morphotropic boundary, as can be seen in Fig. 10. The general dielectric behavior of the near-morphotropic 80/20 composition and the two bronze end members, PKN and BNN, are shown as a function of temperature in Fig. 11.



SC5340.6SA

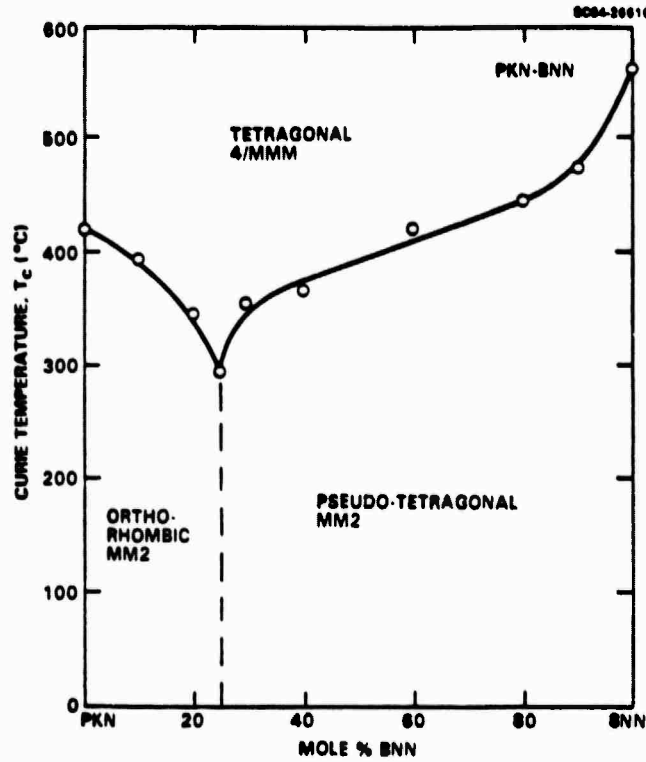


Fig. 9 Morphotropic phase boundary conditions for the system PKN-BNN.

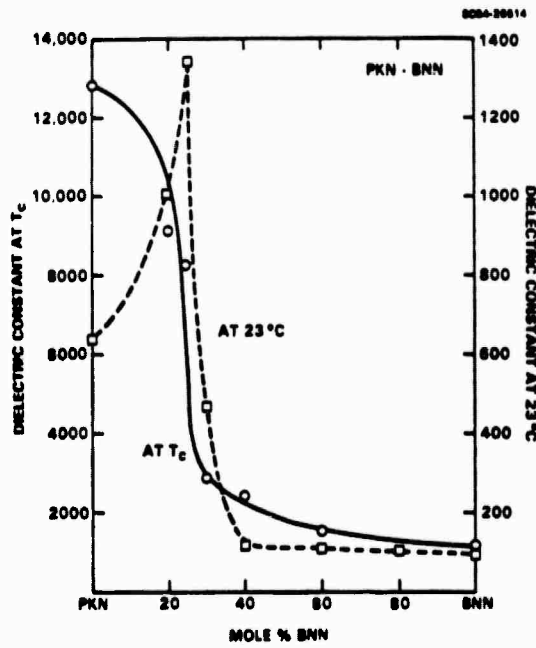


Fig. 10 Dielectric constant (at 10 kHz) vs composition for the system PKN-BNN.

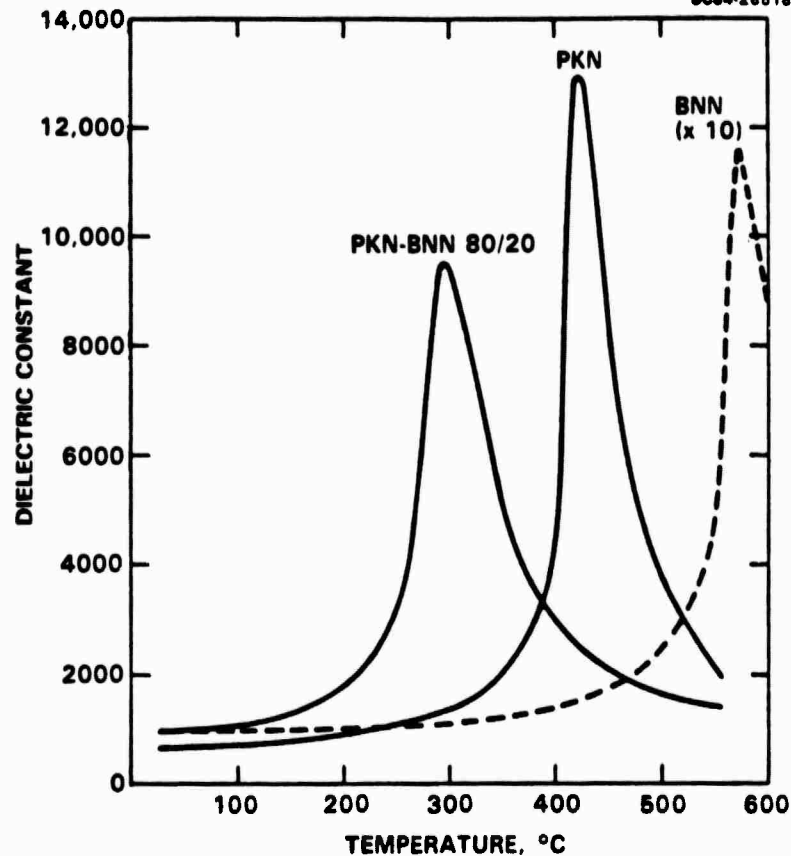


Fig. 11 Dielectric constant of ceramic PKN, 0.8 PKN-0.2 BNN and BNN as a function of temperature. Data for BNN is expanded by a factor of 10 for clarity.

The dramatic changes in the dielectric properties at morphotropy are reflected in the behavior of the lattice parameters as a function of composition, as shown in Fig. 12. These data were obtained by careful least-squares evaluation of powder x-ray diffraction data, with excellent fits being obtained for all compositions. Of particular interest in Fig. 12 is the smooth monotonic decrease in the a lattice parameter, whereas b and c remain constant up to  $x = 0.25$ , at which point an abrupt discontinuity occurs. This dramatic behavior suggests that near-morphotropic compositions in the PKN-BNN system should display particularly enhanced piezoelectric and electro-optic properties.

SC5340.6SA

Both the PKN-BNN and BNN-SNN systems have been shown to be promising for electro-optic, pyroelectric and millimeter wave device application studies. A few compositions exhibit enhanced dielectric properties at room temperature and at  $T_c$ . Some of these will be selected for future single crystal Czochralski growth, and the ferroelectric and electro-optic properties will be established in greater detail.

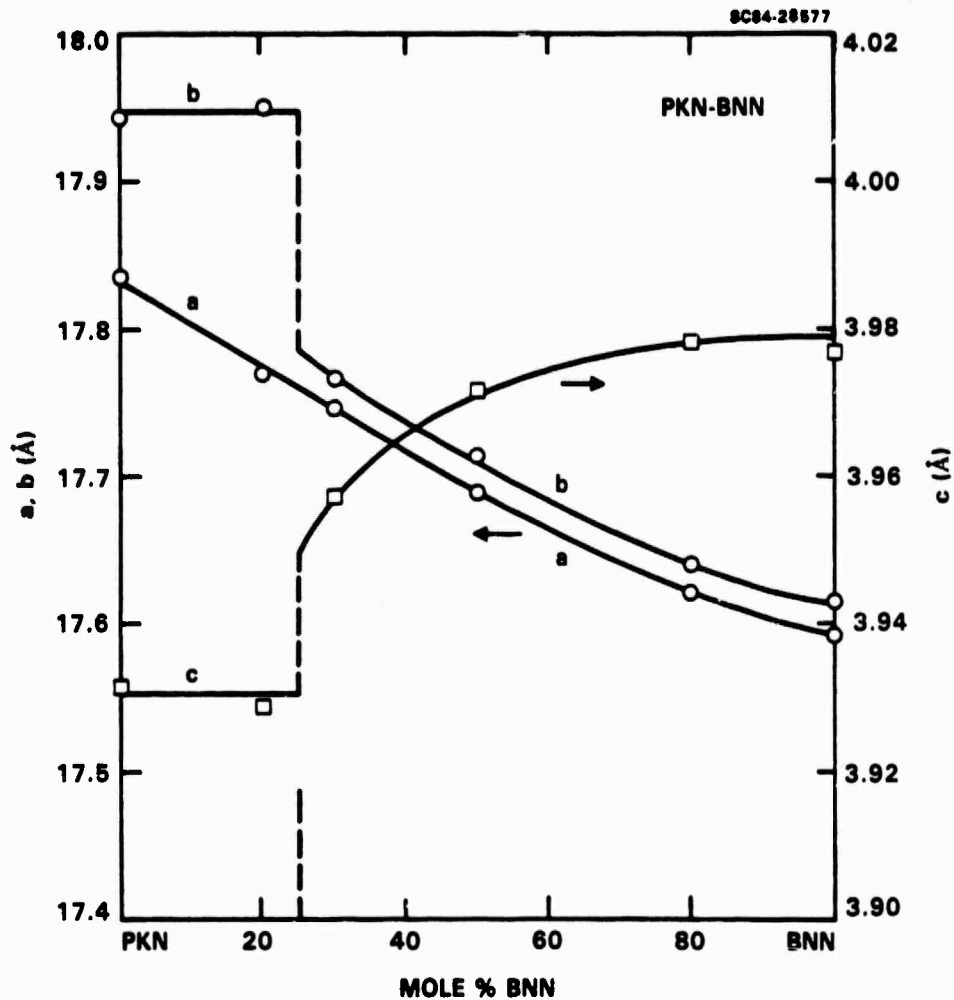


Fig. 12 Structural lattice parameters as a function of composition for PKN-BNN. Note the abrupt discontinuity for the b and c parameters at the morphotropic 0.75 PKN-0.25 BNN composition.



## 5.0 OPTICAL EVALUATION OF PBN

### 5.1 Introduction

The task taken up in the current contract period has been to complement the crystal growth work carried through last period and develop  $Pb_{1-x}Ba_xNb_2O_6$  (PBN) compositions close to morphotropy, but on the orthorhombic side of the phase boundary.

In the family of orthorhombic ferroelectric bronzes in the Shuvalov species  $4/mmm (2)D2F mm2$ , the nonzero polarizations in the ferroelectric phase are  $P_1^2 = P_2^2 \neq 0$ ,  $P_3 = 0$ , and the equations for the spontaneous perturbation of the optical impermeability induced by the phase change at  $T_c$  become

$$\begin{aligned}\Delta R_{11} &= (g_{11} + g_{21})P_1^2 \\ \Delta R_{22} &= (g_{11} + g_{21})P_1^2 \\ \Delta B_{33} &= 2g_{13}P_1^2 \\ \Delta B_{12} &= g_{66}P_1^2 \quad .\end{aligned}\tag{5.1}$$

For the single domain state, the optical indicatrix becomes biaxial with three inequivalent principle indices. In Eq. (5.1), the nonzero  $\Delta B_{12}$  is due to the use of the original prototypic tetragonal axes. Rotating the axial system  $45^\circ$  in the  $ab$  (12) plane eliminates  $\Delta B_{12}$  and destroys the equivalence between  $\Delta B_{11}'$  and  $\Delta B_{22}'$  in the new correct orthorhombic axial system.

Similarly to the tetragonal case, the morphic linear electro-optic  $r$  coefficients are given by



$$\begin{aligned}r_{11} &= r_{22} = 2g_{11}P_1\epsilon_{11} \\r_{12} &= r_{21} = 2g_{21}P_1\epsilon_{11} \\r_{13} &= r_{23} = 2g_{13}P_1\epsilon_{33} \\r_{34} &= r_{35} = 2g_{44}P_1\epsilon_{33} \\r_{16} &= r_{26} = 2g_{44}P_1\epsilon_{11}\end{aligned}\tag{5.2}$$

In the ferroelectric phase, the dielectric stiffness  $\chi_{33}^T$  is given by

$$\chi_{33}^T = 2\alpha_3 + 4\alpha_{13}P_1^2 \quad . \tag{5.3}$$

Because the longitudinal Curie temperature  $\theta_3$  is now close to  $\theta_1$  in compositions on the orthorhombic side but close to morphotropy,  $\alpha_3$  will be negative and increasing with decreasing temperature. The transition at  $T_C$  is, however, first order and thus  $P_1$  is less than parabolic against  $T$ , so that  $\chi_{33}$  will be small and decreasing with  $T$ . Thus,  $\epsilon_{33}$  will be large and increasing with decreasing temperature, leading to large values of  $r_{13}$ ,  $r_{34}$  and  $r_{35}$ .

## 5.2 Exploratory Measurements

A number of PRN crystals have been pulled with compositions increasingly rich in Ba. For a morphotropic composition, ceramic studies suggest that  $T_C \approx 260^\circ\text{C}$ .

In Fig. 13, dielectric data are shown for a poled single crystal region of a composition just in the orthorhombic stability region. It is evident that the transition temperature  $T_C = 268^\circ\text{C}$  is very close to the morphotropic value. The high value of  $K_C$  (the relative permittivity  $\epsilon_{33}$ ), is clearly evident, and the slow increase with decreasing temperature is also evident. The rather small difference between  $K_a$  and  $K_b$  ( $\epsilon_{11}$  and  $\epsilon_{22}$ ) is unexpected and, if confirmed in future measurements, suggest an unusually small value for  $\alpha_{12}$ .

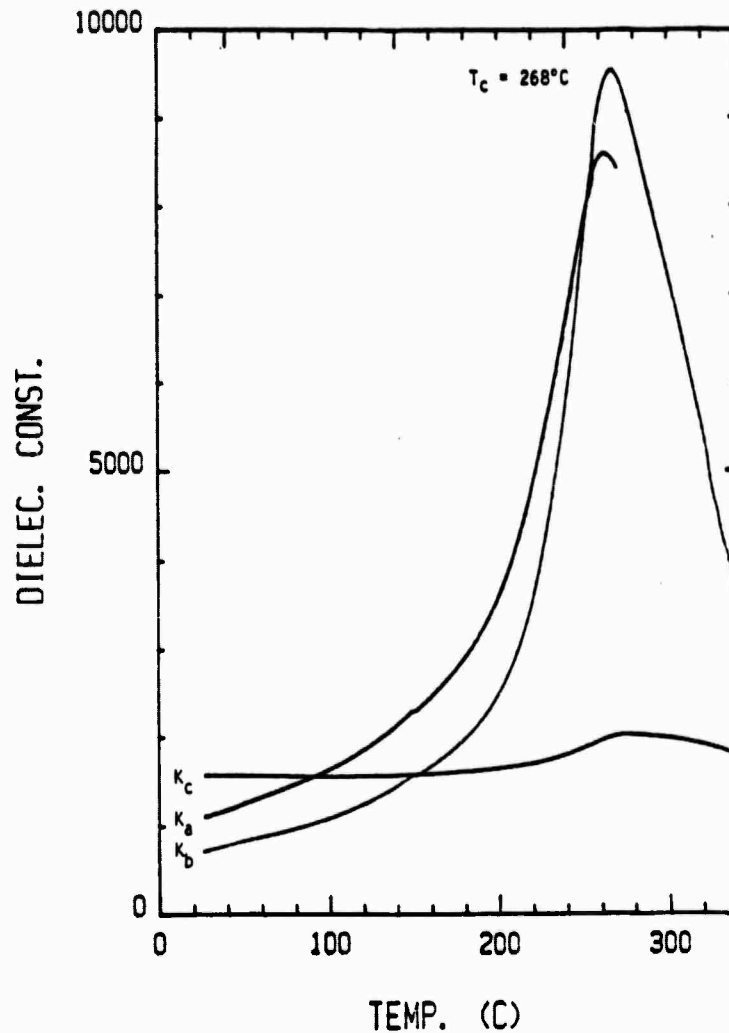


Fig. 13 K vs T measurements along the a, b, c axes of orthorhombic PBN (composition near the morphotropic boundary).

It was gratifying to find that even for compositions very close to the morphotropic boundary, we could find areas quite clear of ferroelastic  $90^\circ$  twins (Fig. 14) and, thus, that we will be able to make measurements of the full family of single domain dielectric, piezoelectric, elastic and electro-optic parameters. A clear confirmation of the quality of the crystal and of



SC5340.6SA

the pure orthorhombic symmetry is given by the conoscopic figure taken in monochromatic NaD light, as shown in Fig. 15. Evidence of the weak biaxial character is as would be expected for a composition close to the MPB.

Current work is concerned with accumulating data upon the single domain properties of these orthorhombic compositions. We are making more detailed measurements of the  $r_{42}$  and  $r_{51}$  coefficients in tetragonal crystals with compositions just on the other side of the MPB, and also preliminary measurements to explore the possibility of forcing the phase change from orthorhombic to tetragonal by using high electric field applied along the crystallographic c-axis.

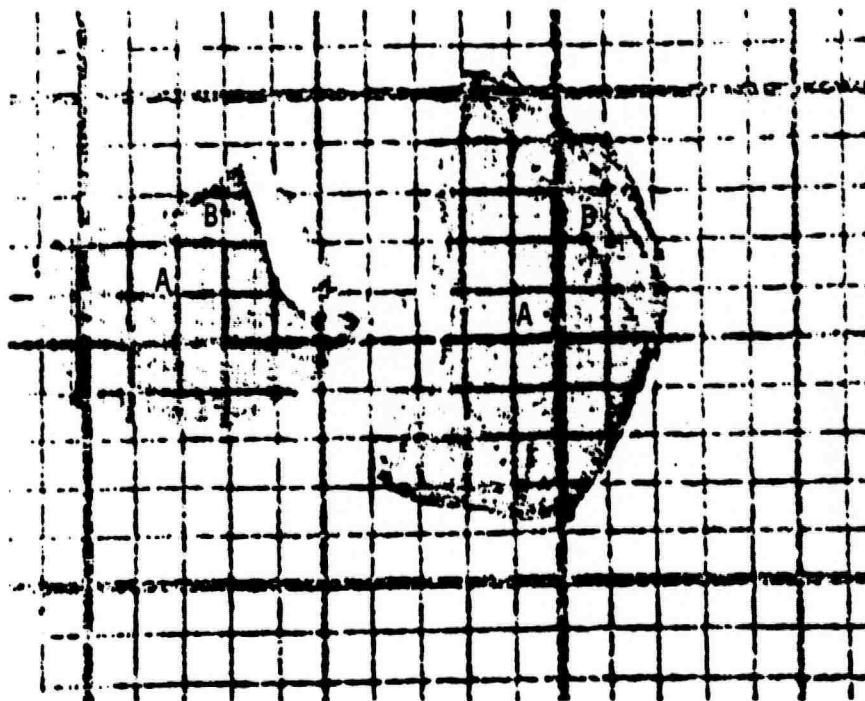


Fig. 14 PBN single crystals of composition near the morphotropic boundary. The large areas (A) are free of  $90^\circ$  domains, (B) show good optical quality of the crystals grown in the composition around  $\text{Pb}_{0.6}\text{Ba}_{0.4}\text{Nb}_2\text{O}_6$ .



Fig. 15 Optical conoscopic figure of orthorhombic PBN, c-plate.



## 6.0 EVALUATION OF THE PHOTOREFRACTIVE EFFECT IN DOPED AND UNDOPED SBN:60

### 6.1 Introduction

The effectiveness of undoped SBN:60, SBN-Fe<sup>3+</sup> (1% by wt.) and SBN-Ce<sup>3+</sup> (0.1% by wt.) as photorefractive media is studied here using the method of two-beam coupling. In particular, the absorption coefficient, the two-beam coupling coefficient, and the writing sensitivity of each crystal is determined, and then used to compare the materials with one another.

Consider the two-wave mixing experiment shown in Fig. 16. Beams 1 and 2 are plane waves which intersect in the crystal and thus form an intensity interference pattern. Charge is excited by this periodic intensity distribution into the conduction band, where it migrates under the influence of

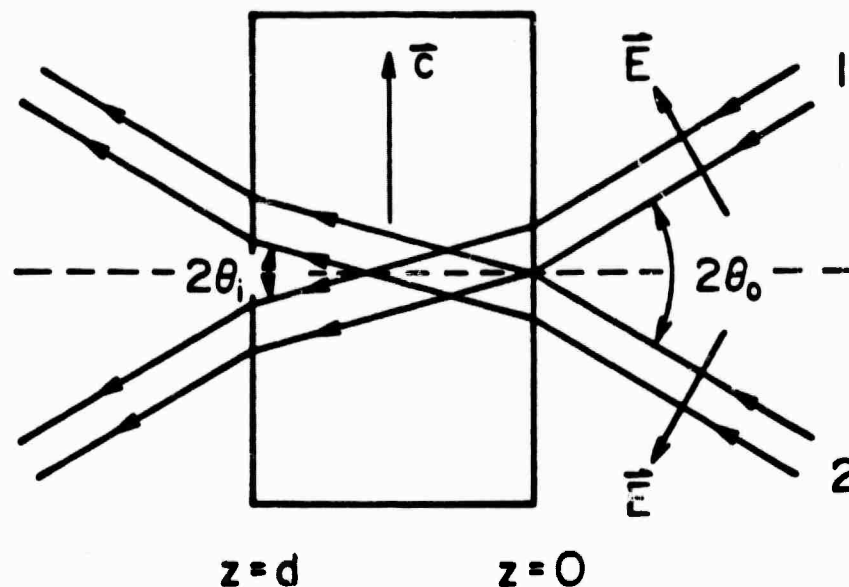


Fig. 16 Experimental setup for two-beam coupling experiments.



SC5340.6SA

diffusion and drift in the internal electric field, and then preferentially recombines with traps in regions of low irradiance. A periodic space-charge is thus created which modulates the refractive index via the electro-optic effect. This index grating, being out of phase with the intensity distribution, introduces an asymmetry that allows one beam to be amplified by constructive interference with light scattered by the grating, while the other beam is attenuated by destructive interference with diffracted light.

Mathematically, this two-beam coupling may be described in the steady-state as follows:

$$\begin{aligned} \frac{dI_1}{d\xi} &= -\gamma \frac{I_1 I_2}{I_1 + I_2} - \alpha I_1 \\ \frac{dI_2}{d\xi} &= \gamma \frac{I_1 I_2}{I_1 + I_2} - \alpha I_2 \end{aligned} \quad (6.1)$$

where  $I_1$  and  $I_2$  are the intensities of beams 1 and 2 inside the crystal,  $\gamma$  is the two-beam coupling coefficient,  $\alpha$  is the absorption coefficient, and  $\xi \equiv z/\cos\theta_i$ , where  $0 < \xi < \lambda \equiv d/\cos\theta_1$ . The transient behavior is modeled by

$$I_i(\xi; t) = (1 - e^{-t/\tau}) I_i(\xi; t \rightarrow \infty) + e^{-t/\tau} I_i(\xi; t = 0), \quad i = 1, 2 \quad (6.2)$$

where  $\tau$  is the characteristic time constant and  $I_i(\xi; t \rightarrow \infty) \equiv I_i(\xi)$ .

The solutions of the above coupled wave equations are

$$\begin{aligned} I_1(\lambda) &= \frac{[I_1(0) + I_2(0)] e^{-\alpha\lambda}}{1 + \frac{I_2(0)}{I_1(0)} e^{\gamma\lambda}} \\ I_2(\lambda) &= \frac{[I_1(0) + I_2(0)] e^{-\alpha\lambda}}{1 + \frac{I_1(0)}{I_2(0)} e^{-\gamma\lambda}} \end{aligned} \quad (6.3)$$



Maximum coupling will, therefore, result in crystals with large  $\gamma$ , but small  $\alpha$ . However,  $\alpha$  and  $\gamma$  are not independent. In fact, since charge must first be excited into a conduction band by the intensity interference pattern in order to start the photorefractive process, some absorption is necessary. This is precisely where the role of the dopant enters. By purposely introducing impurities into the crystal, donor sites are created which become the absorption centers. It must be noted, however, that any absorption which does not contribute to the photorefractive mechanism is undesirable.

## 6.2 Photorefractive Measurements

Figures 17 and 18 show qualitatively the effect of Ce and Fe impurities on the absorption spectra of undoped SBN:60, whose spectra is given in Fig. 19. Several interesting observations can be made. For one, the band edge shifts from 400 nm in SBN to 430 nm in SBN-Ce and 500 nm in SBN-Fe. Secondly, although the SBN in Fig. 19 was not intentionally doped, there are signs of deep level impurities evidenced by perturbations in the spectra near 550 nm. Finally, the effects of Ce and Fe in SBN are seen to be significantly different. While the spectra of SBN-Ce is rather featureless with a broad deep level centered at 480 nm, the spectra of SBN-Fe displays a structured but otherwise broad absorption extending from 500 nm to 700 nm, with characteristic peaks at 500 nm and 590 nm. Future investigation of these lines will indicate whether or not they contribute to the photorefractive effect.

The final quantity of interest, the writing sensitivity  $W$ , defined by  $W \equiv [I_1(0) + I_2(0)]\tau$ , is a measure of the incident energy needed to produce the index grating. Since, in basic photorefractive theory,  $W$  is a constant, the writing sensitivity also serves, therefore, as an indicator of the speed of response of the crystal for arbitrary values of irradiance.

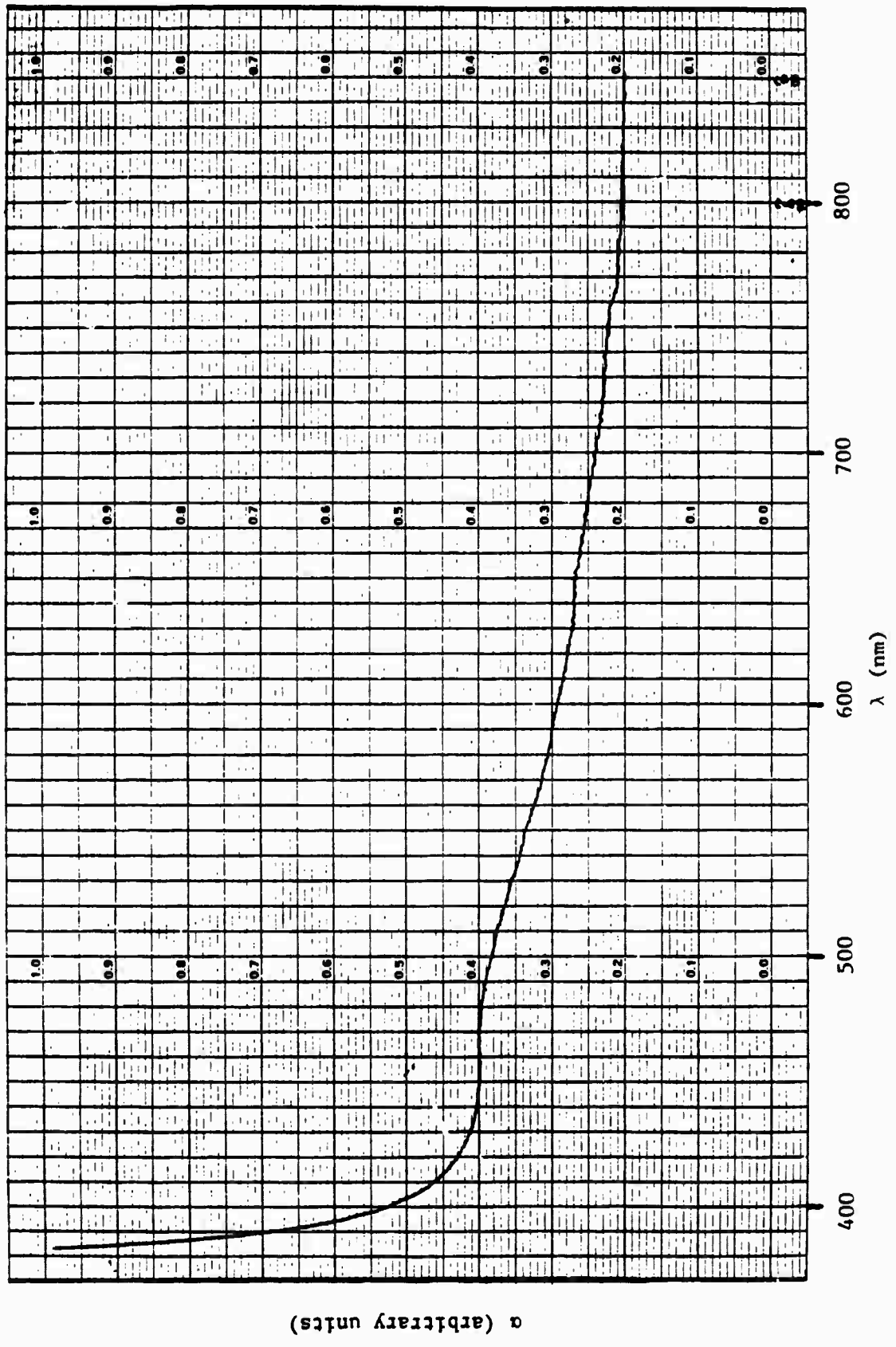


Fig. 17 Absorption spectra of SBN:60-Ce (0.1%)

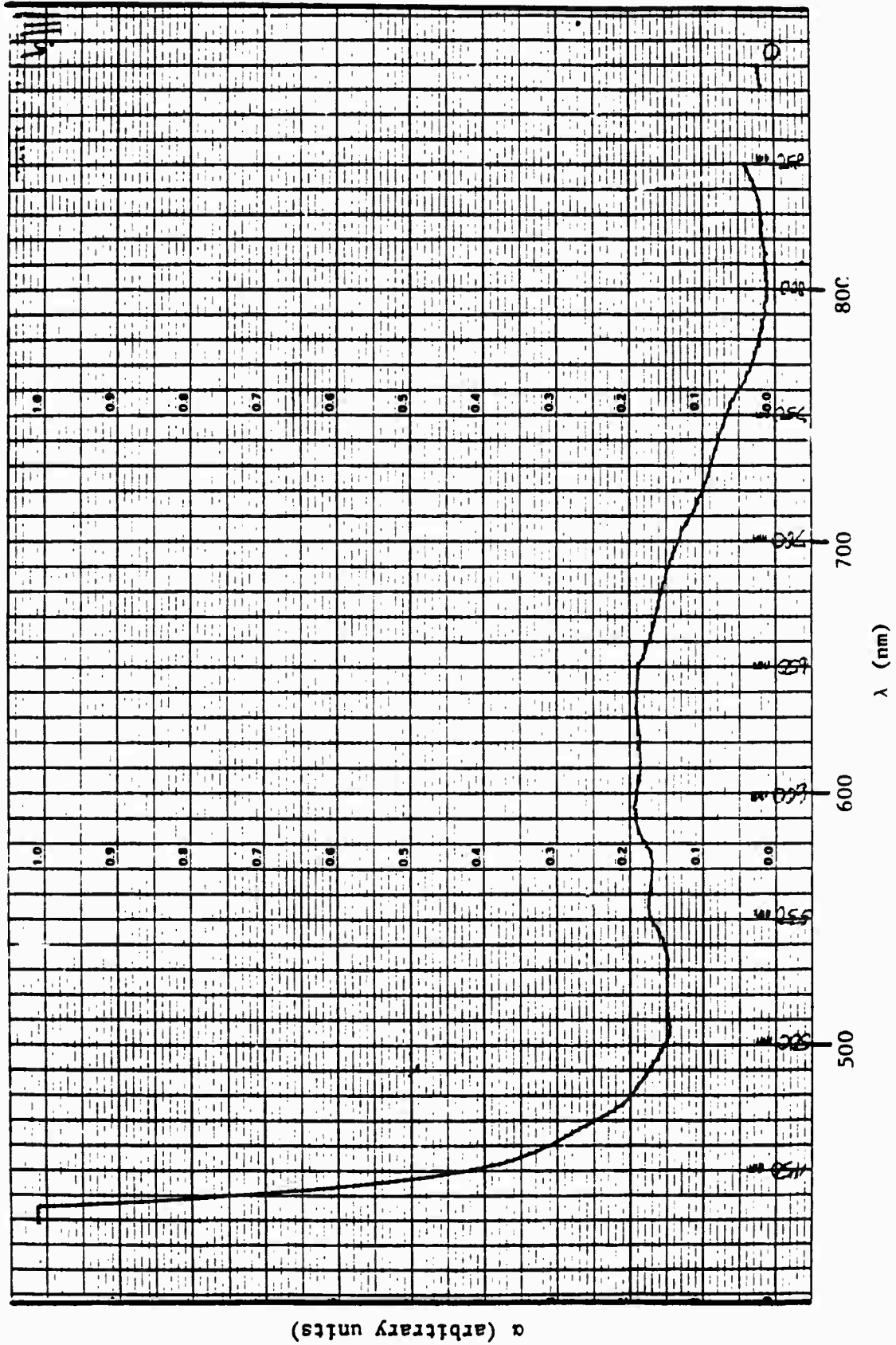


Fig. 18 Absorption spectra of SRN:60-Fe (1.0%).

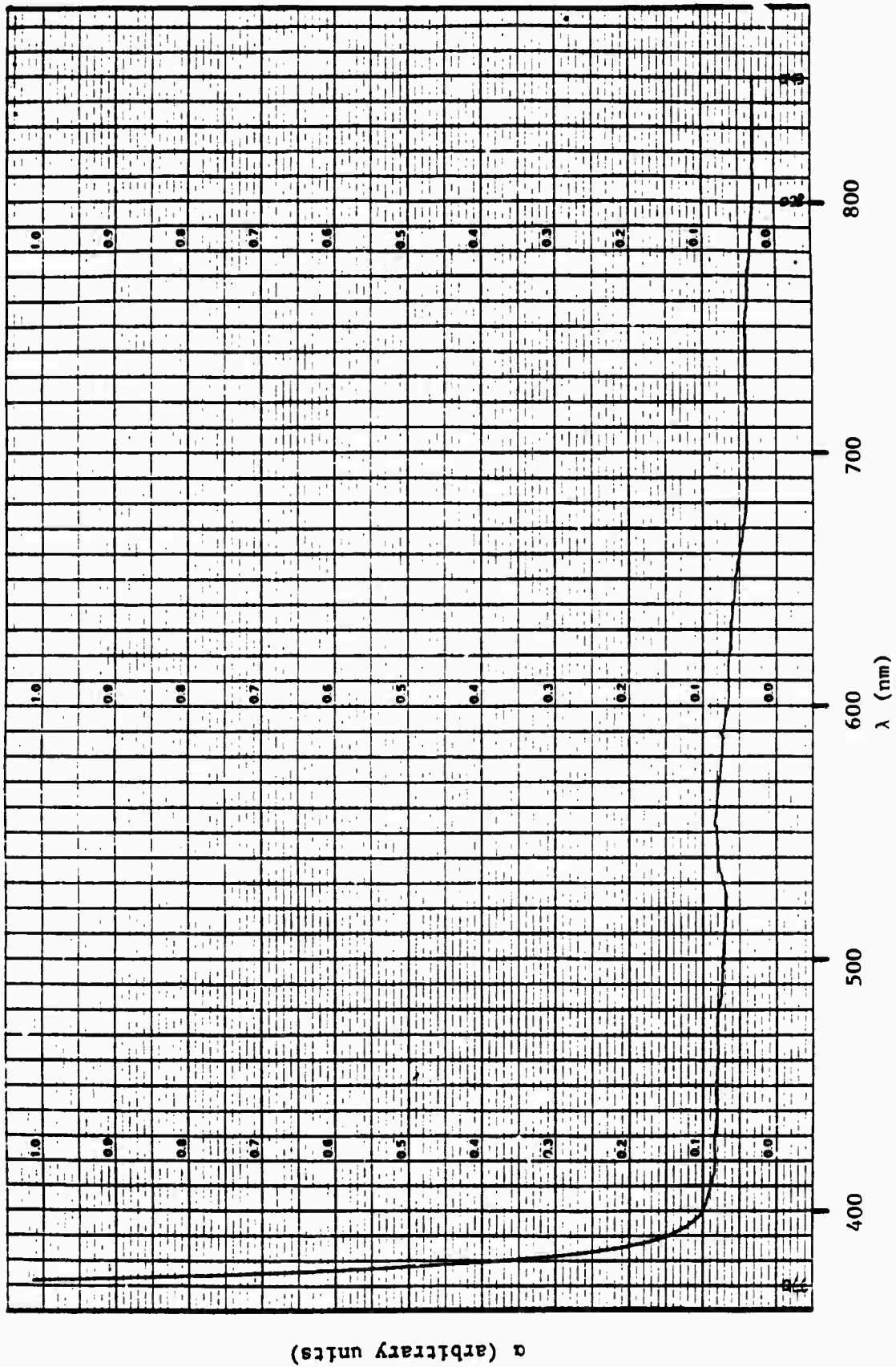


Fig. 19 Absorption spectra of SBN:60



SC5340.6SA

Table 9 summarizes the experimental results for the three materials. Unfortunately, the SBN:60-Fe crystal was excessively doped, which created striations that interfered with measurements of  $\gamma$  and  $\alpha$ . Therefore, only the writing sensitivity was obtained, and was found to be about 25% larger than that of undoped SBN. However, this result should not be used to conclude that doping SBN with Fe results in a slower photorefractive materials, since the quality of the particular SBN-Fe crystal was lower than that of the other two crystals. A crystal with lower Fe content will probably render much better results.

The data in Table 9 indicate that the introduction of Ce into SBN:60 results in a crystal with a larger two-beam coupling coefficient and a better writing sensitivity. However, the absorption coefficient is affected negatively. This increase in absorption may, indeed, be unavoidable, since it probably contributes to the better values of  $\gamma$  and  $W$ . Also, future experimentation with the reduction ratio of SBN-Ce, i.e., the fraction of  $Ce^{3+}$  to  $Ce^{4+}$  in the crystal, may further increase the effectiveness of SBN-Ce as a photorefractive material.

Table 9  
Optical Properties of Doped and Undoped  
SBN:60 Crystals\*

|                              | SBN   | SBN:Ce | SBN:Fe |
|------------------------------|-------|--------|--------|
| $\alpha$ (cm <sup>-1</sup> ) | 0.04  | 1.8    | --     |
| $\gamma$ (cm <sup>-1</sup> ) | 3.0   | 11.0   | --     |
| $W$ (mJ/cm <sup>2</sup> )    | 122.0 | 101.0  | 152.0  |

\* Experimental results for  $2\theta_0 = 15^\circ$ ,  $\lambda = 5145\text{\AA}$ ,  
 $I_1(0) + I_2(0) = 100 \text{ mW/cm}^2$ ,  $I_2(0)/I_1(0) = 2$



## 7.0 FUTURE PLANNED WORK

- Further refine and evaluate the growth of high purity single crystal SBN:60.
- Establish optimum concentrations of Fe and Ce dopants in SBN:60 necessary for improved photorefractive sensitivity and speed.
- Examine the dielectric and optical properties of SBN crystals doped with other cations.
- Establish SBN:75 LPE growth from the SrO-BaO-Nb<sub>2</sub>O<sub>5</sub>-V<sub>2</sub>O<sub>5</sub> flux system.
- Continue development of the BaV<sub>2</sub>O<sub>6</sub>-PBN:60 and Pb<sub>1-x</sub>Ba<sub>x</sub>V<sub>2</sub>O<sub>6</sub>-PBN:60 flux system for LPE growth.
- Attempt single crystal growth of near-morphotropic BNN-SNN and PKN-BNN bronze compositions for dielectric, structural and optical evaluation.
- Continue measurement of the E-O coefficients of near-morphotropic single crystal PBN.



## 8.0 PUBLICATIONS AND PRESENTATIONS

### 8.1 Publications

1. R.R. Neurgaonkar, W.K. Cory and J.R. Oliver, "Growth and Applications of Ferroelectric Tungsten Bronze Family Crystals," *Ferroelectrics* 51, 3 (1983).
2. R.R. Neurgaonkar, J.R. Oliver and L.E. Cross, "Ferroelectric Properties of Tetragonal Tungsten Bronze Single Crystals," *Ferroelectrics* 56, 31 (1984).
3. T.R. Shrout, L.E. Cross and D.A. Hukin, "Ferroelectric Properties of Tungsten Bronze Lead Barium Niobate (PBN) Single Crystals," to be published in *Ferroelectrics*.

### 8.2 Presentations

1. R.R. Neurgaonkar, W.K. Cory and J.R. Oliver, "Growth and Applications of Tungsten Bronze Family Crystals," presented at the 1983 IEEE Int. Symp. on Applications of Ferroelectrics, June 1-3, 1983, Gaithersburg, MD.
2. R.R. Neurgaonkar, J.R. Oliver and L.E. Cross, "Growth and Application of Ferroelectric Tungsten Bronze Family Crystals," presented at the 5th European Meeting on Ferroelectrics, Sept. 26-30, 1983, Benalmadena, Spain.
3. T.R. Shrout, H.C. Chen and L.E. Cross, "Dielectric and Piezoelectric Properties of Tungsten Bronze Lead Barium Niobate ( $Pb_{1-x}Ba_xV_2O_6$ ) Single Crystals," presented at the 5th European Meeting on Ferroelectrics, Sept. 26-30, 1983, Benalmadena, Spain.
4. J.R. Oliver and R.R. Neurgaonkar, "Ferroelectric Solid Solutions Based on the Tungsten Bronze Structure," presented at the 86th Annual Meeting of the Am. Ceram. Soc., April 30-18, 1984, Pittsburgh, PA (invited paper).
5. J.R. Oliver and R.R. Neurgaonkar, "Morphotropic Tungsten Bronze Solid Solutions," accepted for presentation at the 37th Pacific Coast Regional Meeting of the Am. Ceram. Soc., October 28-31, 1984, San Francisco, CA.
6. R.R. Neurgaonkar, W.K. Cory and J.R. Oliver, "Ferroelectric Tetragonal Tungsten Bronze Crystals for Optoelectronic Applications," accepted for presentation at the 37th Pacific Coast Regional Meeting of the Am. Ceram. Soc., October 28-31, 1984, San Francisco, CA.



SC5340.6SA

#### 9.0 REFERENCES

1. U.V. Voronov, I.R. Dorosh, Y.S. Kusiminov and N.V. Tkachenko, Sov. J. Quantum Electronics 10, 1346 (1980).
2. K. Megumi, H. Kozuka, M. Kobayashi and Y. Furuhashi, Appl. Phys. Lett. 30, 631 (1977).
3. J.E. Geusic, A.J. Levenstein, J.J. Rubin, S. Singh and L.G. Van Uitert, Appl. Phys. Lett. 11, 269 (1967).
4. R.L. Barus, J. Appl. Cryst. 1, 290 (1968).
5. R.R. Neurgaonkar and L.E. Cross, Final Report (DARPA), Contract No. F49620-78-C-0093 (1982).
6. K. Nagata, T. Yamazaki and K. Okazaki, Proc. 2nd Int. Meeting on Ferroelectric Materials and Their Applications, 251 (1979).